Parity violation in molecular magnetic resonance properties

Dissertation for the degree of Doctor Philosophiae

Ville Weijo
University of Helsinki
Department of Chemistry
Laboratory of Physical Chemistry
P. O. Box 55
FI-00014 University of Helsinki, Finland

To be presented, with the assent of the Faculty of Science, University of Helsinki, for public discussion in Auditorium A110, Department of Chemistry (A. I. Virtasen aukio 1, Helsinki), August 22nd, 2008, at noon.

Helsinki 2008

Supervised by

Doc. Pekka Manninen
Department of Chemistry
University of Helsinki
and
CSC, the Finnish IT Center for Science

Reviewed by

Prof. Kari Laasonen
Department of Chemistry
University of Oulu

Prof. Peter Schwerdtfeger
Centre of Theoretical Chemistry and Physics
The New Zealand Institute for Advanced Study

ISBN 978-952-92-4260-3 (paperback)
ISBN 978-952-10-4873-9 (PDF)
http://ethesis.helsinki.fi

Yliopistopaino Helsinki 2008

Contents

List of publications

Publications included in the thesis with author's contribution

I. V. Weijo, P. Manninen and J. Vaara, **"Perturbational calculations of parity-violating effects in nuclear-magnetic-resonance parameters"**, *J. Chem. Phys.* **123**, 054501 (2005).

II. V. Weijo, R. Bast, P. Manninen, T. Saue and J. Vaara, **"Methodological aspects in the calculation of parity-violating effects in nuclear magnetic resonance parameters"**, *J. Chem. Phys.* **126**, 074107 (2007).

III. V. Weijo, M. Bo Hansen, O. Christiansen and P. Manninen, **"The role of vibrational effects in calculation of parity-violating contributions to the nuclear magnetic resonance shielding"**, *submitted for publication*.

IV. V. Weijo, P. Manninen and J. Vaara, **"Effect of molecular size on the parity-non-conserving contributions to the nuclear magnetic resonance shielding constant"**, *Theor. Chem. Accounts* (2008), DOI: 10.1007/s00214-008-0447-2.

V. V. Weijo and P. Manninen, **"Parity-violating effects in electron spin resonance g-tensors"**, *Chem. Phys. Lett.* **433**, 37 (2006).

The author participated in planning and the formulation of theory in every article, carried out all or most of the calculations, except in Paper II, where R. Bast completed approximately half of the calculations. The author wrote the first draft of every article, and they were completed as teamwork.

Other publications

- V. Weijo, P. Manninen, P. Jørgensen, O. Christiansen and J. Olsen, **"General biorthogonal projected bases as applied to second-order Møller–Plesset perturbation theory"**, *J. Chem. Phys.* **127**, 074106 (2007).

- M. Ziółkowski, V. Weijo, P. Jørgensen, O. Christiansen and J. Olsen, **"Minimal residual methods. An analysis and applications to atomic-orbital coupled-cluster theory"**, *J. Chem. Phys.* **128** , 204105 (2008).

Acknowledgements

Research for this thesis has been formally done in association with the Laboratory of Physical Chemistry (University of Helsinki) during the years 2005-2008. I would like to express my greatest gratitude to my supervisor, Pekka Manninen. He has given me space to do things my way, and when the things have not been working very well, he has had encouraging words to spare. He has arranged opportunities for me to work abroad and see the world, and also, opportunities to discuss about topics related and unrelated to science in formal and informal environments with him.

I would also like to thank Juha Vaara for bringing me into quantum chemistry during my M.Sc. studies. He has also co-authored several of the papers included in thesis, and his very careful approach has been very helpful (and saved us from a catastrophe or two). I am also grateful for my other co-authors Radovan Bast and Trond Saue from the Université Louis Pasteur (Strasbourg) and Mikkel Bo Hansen and Ove Christiansen from the University of Århus.

Most of the time during my Ph.D. studies I spent in Århus, where Poul, Jeppe and Ove introduced me to the deeper secrets of electronic structure theory. Their ”finding problems from where there were none” approach to science made a great impression on me. From Århus, I would like to thank my colleagues Marcin, Peter, Thomas, Stinne, Mikkel, Daniele, Brano and Anna for making my stay pleasant. I acknowledge my former fellow M.Sc. students from the laboratory of physical chemistry, and also people from the Swedish teaching laboratory I occasionally met. From there, Michael Patzschke and Mikael Johansson deserve a big thanks for their language related comments on this thesis.

Not all the life is related to science. I would especially like thank my former flatmates very much for their contributions to my well-being. Also, my family and friends from Lappeenranta (and Helsinki) helped me to be the man I am today and I am grateful for that.

Helsinki, August 2008
Ville Weijo

1 Introduction

Classical and quantum electrodynamics (QED) do not discriminate between a molecule and its mirror image. From the electrodynamics perspective, the two CHFClBr molecules in Figure 1.1 have the same bond lengths, bond angles and energy levels, although it is impossible to place the other molecule exactly on top of the other only by rotating them. The molecules are mirror images of each other, i.e., if the x-axis is reversed in the other picture, then the molecules can be rotated to overlap exactly.

In nature, however, not all interactions are as indiscriminative as electrodynamics. In the early days of particle physics, it was thought that the mirror image symmetry, or parity, is conserved under all interactions. The so-called weak interaction was postulated in 1949 to explain certain decays of nuclei, and like all the previously known interactions, it was thought to be parity conserving. In 1956, Lee and Yang proposed two experiments to actually test the

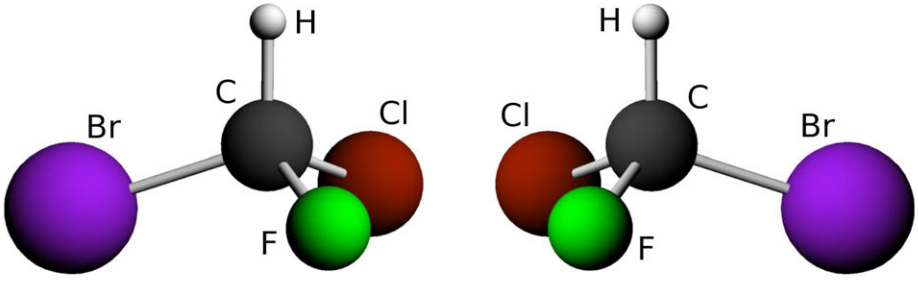

Figure 1.1: Two enantiomers of the CHFClBr molecule. Molecule on the left is the S-enantiomer and the right one is the R-enantiomer.

conservation of parity in weak interactions [1]. In the first experiment, the β decay of the ^{60}Co nucleus in a homogeneous magnetic field (to orientate the nuclear spin) was to be examined; an asymmetry in the electron momentum distribution with respect to the nuclear orientation would have been a definite sign for the parity violation. In the other proposed experiment, it was proposed to detect parity violating (PV) effects in the π meson decay. Half a year later, both experiments were realized and the parity violation was detected [2, 3]. Lee and Yang shared the Nobel prize in Physics for their groundbreaking suggestions in 1957.

The theory of parity-violating weak interactions was formulated more rigorously by Feynman and Gell–Mann [4] and by Sudarshan and Marshak [5], who based it on point-like interactions (or Fermi's interaction). This so called V-A theory (a vector current coupled with an axial vector current) is not, however, renormalizable (at least in the QED sense) and it leads to incurable divergences. Several years later, both QED and weak interaction were unified under the electro-weak (EW) gauge theory. This new theory was, as it turned out, renormalizable ('t Hooft and Veltman, Nobel prize in 1999) and it predicted a neutral parity-violating current that is mediated by a new Z^0 boson [6], among other things. For their part in developing EW theory, Glashow, Salam and Weinberg shared a Nobel prize in 1979. The Z^0 boson was directly observed in CERN in 1983, and subsequently Rubbia and van der Meer shared a Nobel prize in 1984 for their contributions to the experiment. But unlike the charged currents that were present in the decays of particles, Z^0 does not alter the charge (or more commonly, the composition) of matter.

From the perspective of the weak interaction and particularly the Z^0 boson, the molecules in Figure 1.1 would not be equal in their bond lengths, bond angles nor energy levels. Influence of the Z^0 boson breaks the degeneracy of energy levels of the enantiomers, shifting the ground state energy of the S-enantiomer down by approximately 1.4×10^{-14} kJ mol^{-1} and that of the R-enantiomer up by the same amount [7], thus making one form energetically more favorable than the other. The existence of energy differences due to PV, albeit very small, gives rise to an interesting question about the origin of the biomolecular homochirality. In nature, biologically relevant chiral molecules are usually encountered in one enantiomeric form (e.g., L-form

for amino acids) only, and if these molecules are synthesized in a laboratory, both forms are produced in equal amounts. From theoretical studies (see Refs. [8, 9] and references therein) it has been found that if the weak interaction is taken into account, usually the forms encountered in nature are energetically more favorable. These findings, however, have been questioned for certain amino acids [10–12]. The smallness of energy differences between amino acids implies that the preference for the lower-energy form due to the parity-violating interaction would produce an excess of one in 10^{17} molecules at room temperature [13]. This is too little to prove a link between biomolecular homochirality and the weak interaction (first suggested by Yamagata in 1966 [14]). However, several models have been established that require only a small energy difference and over time, one enantiomer would dominate the other [13, 15, 16]. These models have received both theoretical and experimental votes for [8, 17, 18] and against [9, 12, 19, 20]. Most of the critique stems from the fact that the conditions of origin of life as well as autocatalytic mechanisms required by the models are unknown. Also, realistic conditions involve other molecules, surfaces etc. that affect catalysis greatly. Thus, Yamagata's hypothesis remains unproven and somewhat unlikely.

The ground state energy differences are not the best candidates for actually observing parity-violating effects in molecules as they are not directly observable. Perhaps closest to a successful experimental observation are differences in vibrational frequencies. Vibrational (and rotational) frequencies of a molecule depend on potential energy surfaces (PES), and thus, if there is a difference in ground state energy between enantiomers, the PESs of those molecules are also different. Parity violation would manifest itself in a mixture of both enantiomers by splitting the vibrational (and rotational) resonance peaks into two, i.e., shifting the vibrational frequencies of enantiomers to different directions by the same amount. Popular molecules for both theoretical and experimental vibrational studies have been chiral halomethanes, such as in Figure 1.1. Theoretical studies for halomethanes containing C, H, F, Cl, Br and I have predicted PV induced splits in the experimentally important C–F stretching mode of less than 0.1 Hz [7, 21–25]. The experimental vibration-rotation resolution in the C–F stretching vibrational band in CHFClBr is roughly 10 Hz at the moment [26, 27], and thus far larger than

predicted splittings. However, several theoretical compounds have been predicted, where the splitting is of the order of 10 Hz [25, 28], but their stability and synthetizability are questionable.

Besides the *tour de force* of observing parity-violation in molecules and the corresponding bragging rights, accurate measurements on the molecular scale could, perhaps surprisingly, improve our knowledge on nuclear and particle physics. Experimental parameters of the weak interaction would be available for examination in measurements (if everything else can be calculated accurately), although the parameters have been measured accurately in high-energy experiments [29]. Also, sensitive experiments can set constraints to models beyond the Standard Model [30]. Perhaps a more realistic application, however, would be in the structure of nuclei and emergence of the PV nucleon-electron interaction. Of specific interest to nuclear physics would be the nuclear anapole moment that has been measured only for ^{133}Cs [31, 32]. At the atomic and molecular levels, the anapole moment is indistinguishable from the spin-dependent PV interaction mediated by the Z^0 boson.

Parity violation in nuclear magnetic resonance (NMR) spectral parameters and computational aspects of their evaluation are the main topics of this thesis. NMR spectroscopy probes the effect of electronic structure on the nuclear spin, and thus could provide a way to observe nuclear spin-dependent PV interactions. Relativistic and non-relativistic theories have been sketched for PV effects in NMR shielding, nuclear spin-spin coupling and spin-rotation tensors, and PV effects in NMR shielding constant have been evaluated using semi-empirical methods [33–35] for more than 20 years. The first *ab initio* calculations of PV shielding constant contributions were made by Laubender and Berger [36] and by Soncini, Faglioni and Lazzeretti [37]. Their results were congruent with each other, and several orders of magnitude smaller than experimental limits. The results were also somewhat smaller than those obtained by semi-empirical methods, but this was due to the relatively light nuclei used in the *ab initio* calculations.

In Paper I of this thesis, the earlier non-relativistic theory for parity violating effects in NMR spectral parameters has been revised and completed. Sample calculations were made for PV nuclear shielding and spin-spin coupling contributions in CHFClBr and CHFBrI. In Paper II, the effects of special

relativity, electron correlation and the choice of the one-electron basis set to the PV contributions are examined in detail (see also Refs. [38] and [39]). To conclude the "sole molecule in vacuum" model, vibrational averaging of PV shielding contributions is considered in Paper III. The dependence of the PV shielding contribution on the size of the molecule is examined in Paper IV in an enantiomeric pair of polysilyenes. An experimental observation of a difference in the shielding constants of ^{29}Si between the enantiomers of the same polysilyenes [40] is also discussed in Paper IV. The difference is several orders of magnitude larger than estimates, and is unlikely to be of the PV origin. In Paper V, the non-relativistic theory of PV effects on the electron spin resonance *g*-tensor was considered for the first time and evaluated for chiral spin-doublet radicals. Although chiral doublet systems are hard to come by, the *g*-tensor could be, in some respect, a better choice for observing PV effects in molecules than NMR methods.

The thesis is laid out as follows: First, we will introduce the low-energy limit of the Z^0 boson exchange and its non-relativistic limit in Chapter 2. In Chapter 3, computational tools for electronic and vibrational structure are briefly introduced. These are applied in Chapter 4, where the results of Papers I–V are summarized. The theories for parity violating effects for NMR and ESR properties are also included in Chapter 4. Finally, in Chapter 5, a short review is presented and possible future prospects are discussed.

2 Mechanism of parity violation and related molecular Hamiltonians

2.1 Parity as a conserved quantity

Before we start to consider what parity violation means, it is good to examine the actual meaning of parity first. Parity transformation changes position vectors $\mathbf{x} \rightarrow -\mathbf{x}$, i.e., mirrors the system. If the Hamiltonian is invariant under the parity transformation P, i.e., it commutes with the parity operator, the total parity of the system is conserved. For example, the basic non-relativistic spin-free many-electron molecular Hamiltonian,[†]

$$H = \sum_i \frac{p_i^2}{2} + \sum_{i<j} \frac{1}{|\mathbf{r}_i - \mathbf{r}_j|} - \sum_{i,K} \frac{Z_K}{|\mathbf{r}_i - \mathbf{r}_K|}, \tag{2.1}$$

where indices i and j refer to electrons and K to nuclei, is invariant under parity transformation. The momentum operator $\mathbf{p}$ changes its sign under the parity transformation (because $\mathbf{p} = -\mathrm{i}\partial/\partial\mathbf{x}$) but its square is unaffected. The electric potential depends only on the distance of two electrons, and consequently, it does not change if the coordinate system is reversed. Naturally, two sequential parity operations brings the system to its initial state, $P^2 = 1$. The consequence of this is that eigenvalues of the parity operator are either $+1$ or -1. The parity of the system is multiplicative, i.e., parities of subsystems are multiplied together to obtain the total parity. Also, particles can have def-

[†]SI -based atomic units are used throughout this work. In atomic units $\hbar = 1$, $m_e = 1$, $e = 1$, $c = 1/\alpha$, $\mu_B = 1/2$ and $1/4\pi\varepsilon_0 = 1$.

inite "internal" parities. For example, spin-$\frac{1}{2}$ fermions (including electrons) are defined to have $+1$ parity and photons to have -1 parity. Parities of other particles can be found from any particle physics textbook.

As an example of a parity-conserving process, we examine an excitation process of an electron to an excited state by a photon. The total parity in the beginning is -1 (photon) $\times$ $+1$ (electron) $\times$ n_i (parity of the spatial part of the initial electron wave function) $= -n_i$. In the final state, we have $+1$ (electron) $\times$ n_f (parity of the final state spatial wave function) $= n_f$. If the parity is to be conserved, parities of the initial and final electron spatial wave functions must be different, $n_i = -n_f$, as can be expected from the electric dipole selection rules. These parity selection rules were initially observed from atomic spectra by Laporte and Meggers [41], and hence are called the Laporte rules in chemistry.

2.2 Electro-weak interaction

Quantum electrodynamics (QED) and the early theory of weak interactions were originally separate theories. The problem with the weak interaction is that its gauge bosons (particles that mediate interactions) are massive, unlike in "normal" gauge theories with only massless gauge bosons. Glashow, Salam and Weinberg devised so called spontaneous symmetry breaking mechanics to incorporate massiveness.

The symmetry of a system can be decomposed into two parts, that of the Lagrangian and that of the vacuum. The Lagrangian describes the equations of motion, and it is the invariance of the Lagrangian that is usually meant when it is said that a system is invariant under some transformation. Vacuum can be invariant under the same transformation or not. If the vacuum is invariant, then the Lagrangian is also invariant and the symmetry is exact. If both of them are non-invariant, the symmetry is explicitly broken. However, if the vacuum is non-invariant (meaning that there are several degenerate vacuum states) then the Lagrangian can still be invariant. By choosing one of the equally good (degenerate) vacuum states in a clever way, it is possible to separate the degrees of freedom in the Lagrangian and new information can be extracted. In this mechanism, the symmetry is said to be spontaneously

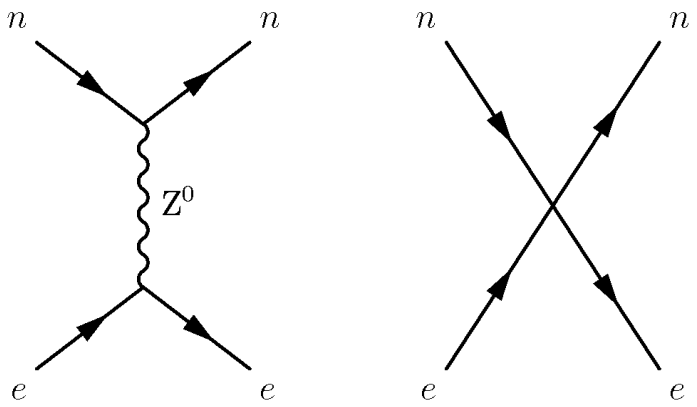

Figure 2.1: Left: The exchange of the Z^0 boson between an electron and a nucleon. Right: Low-energy limit of the interaction on the left.

broken.

In the case of the EW interaction, the initial $SU(2) \times U(1)$ gauge symmetry with 3+1 massless gauge bosons is turned in the spontaneous symmetry breaking to a residual $U(1)$ symmetry with only one massless boson. The three other gauge bosons acquire mass, and these are the W^+, W^- and Z^0 bosons. The remaining massless gauge boson is the photon as we know it. Of the massive gauge bosons W^+ and W^- for instance change the structure of nuclei, i.e., change protons to neutrons and vice versa and are present in radioactive decay processes. The Z^0 boson is chargeless and the structure of matter is unaffected by it.

2.3 Low-energy limit of the Z^0 exchange

Of special interest in this thesis is the exchange of the Z^0 boson between nucleons and electrons in molecules. To an accuracy of one per cent (we will come to this later), we can approximate this interaction by a second-order perturbation theory expression. The perturbation theory diagram for the leading-order interaction is shown left in Figure 2.1. The Z^0 boson is very massive, and the momentum transferred in the interaction is small in the low-

energy limit that is sufficient for molecules. This reduces the exchange of the Z^0 boson to a contact-like interaction illustrated on the right in Figure 2.1. An effective Hamiltonian density of this interaction is [42–44]

$$\mathcal{H}^{\mathrm{PV}}(x) = \frac{G_F}{\sqrt{2}} J_\mu^{(h)}(x) J_\mu^{(l)}(x), \tag{2.2}$$

where $J_\mu^{(l)}(x)$ and $J_\mu^{(h)}(x)$ are leptonic and hadronic currents, respectively, and G_F is the Fermi coupling constant. The leptonic part is

$$J_\mu^{(l)}(x) = -\frac{1}{2}\left[(1-4\sin^2\theta_W)\bar{e}(x)\gamma_\mu e(x) - \bar{e}(x)\gamma_\mu\gamma_5 e(x)\right], \tag{2.3}$$

where $e(x)$ is the electron field and $\bar{e}(x) = e^\dagger(x)\gamma_0$ [42–44]. γ_μ are the gamma matrices (see, e.g., Ref. [44]). For convenience, the interactions between electrons and quarks in a nucleon are combined and treated as one effective interaction. The result is the hadronic current [42–44]

$$J_\mu^{(h)}(x) = \bar{N}(x)\gamma_\mu(1-\gamma_5)\frac{\tau_3}{2}N(x) - 2\sin^2\theta_W \bar{N}(x)\gamma_\mu\frac{1+\tau_3}{2}N(x). \tag{2.4}$$

A nucleon field is described by $N(x)$, in which protons and neutrons are arranged in an isospin doublet. The isospin operator τ_3 is similar to the Pauli spin-operator σ_3, and it gives the prefactors $+1$ and -1 for protons and neutrons, respectively.

Terms containing γ_μ behave like vectors (V) in parity transformations and terms containing $\gamma_\mu\gamma_5$ behave like axial vectors (A). The currents (2.3) and (2.4) divide the total interaction Hamiltonian into four types of combinations, V^e-V^h (meaning the interaction of vector parts of both electronic and hadronic currents) V^e-A^h, A^e-V^h and A^e-A^h. From these, the A^e-V^h and V^e-A^h currents violate the parity conservation, and these are the ones we are interested in after a few further approximations.

Although intra-nuclear forces are strong, it seems that a non-relativistic approximation can be used for nucleons [45]. The non-relativistic limit of the wave function can be written as [42]

$$\psi(x) = \begin{pmatrix} \varphi(x) \\ \frac{\boldsymbol{\sigma}\cdot\mathbf{p}}{2m}\varphi(x) \end{pmatrix}, \tag{2.5}$$

where $\varphi(x)$ is a non-relativistic two-component wave function. m and σ are the mass and the spin-operator of the nucleus, respectively. With these approximations for interaction and nucleon energies, we can start to investigate different combinations of currents (2.3) and (2.4).

Let us first consider the $\mu = 0$ part of the hadronic axial-vector-current interaction in the non-relativistic approximation and its matrix element

$$\begin{aligned}\langle a|N^\dagger(x)\gamma_0\gamma_0\gamma_5 N(x)|a\rangle &= \psi_a^*(x)\gamma_5\psi_a(x)\\ &= \varphi_a^*(x)\left(\frac{\sigma\cdot\mathbf{p}}{2m}\varphi_a(x)\right)\\ &\quad+\left(\frac{\sigma\cdot\mathbf{p}}{2m}\varphi_a(x)\right)^\dagger\varphi_a(x).\end{aligned}\tag{2.6}$$

In the non-relativistic approximation, the matrix element contains a $\alpha^2 p/m \ll 1$ factor, and thus it should be small. For example, in ^{133}Cs the matrix element is even further suppressed by considerations of the nuclear model, and is approximated to be of the order of per mille as compared to other terms [45]. By these considerations, terms containing elements like Eq. (2.6) can be neglected.

The same interaction with $\mu = 1, 2, 3$ are described by

$$\begin{aligned}\langle a|N^\dagger(x)\gamma_0\gamma_\mu\gamma_5 N(x)|a\rangle &= \psi_a^*(x)\gamma_0\gamma_\mu\gamma_5\psi_a(x)\\ &= \psi_a^*(x)\begin{pmatrix}\sigma_\mu & 0\\ 0 & \sigma_\mu\end{pmatrix}\psi_a(x)\\ &= \varphi_a^*(x)\sigma_\mu\varphi_a(x)\\ &\quad+\left(\frac{\sigma\cdot\mathbf{p}}{2m}\varphi_a(x)\right)^*\sigma_\mu\frac{\sigma\cdot\mathbf{p}}{2m}\varphi_a(x).\end{aligned}\tag{2.7}$$

The second part of the expression (2.7) is again suppressed by the $\alpha^2 p/m$ terms. The first part, however, is not and it will provide us with a nuclear-spin-dependent effective interaction.

The matrix elements of the vector part of the current are simpler. The $\mu = 0$ term has the following simple expression

$$\langle a|N^\dagger(x)\gamma_0\gamma_0 N(x)|a\rangle = \psi_a^*(x)\psi_a(x),\tag{2.8}$$

whereas the part with $\mu = 1, 2, 3$ are of the following form,

$$\begin{aligned}\langle a|N^\dagger(x)\gamma_0\gamma_\mu\gamma_5 N(x)|a\rangle &= \psi_a^*(x)\gamma_0\gamma_\mu\gamma_5\psi_a(x)\\ &= \psi_a^*(x)\begin{pmatrix}0 & \sigma_\mu\\ \sigma_\mu & 0\end{pmatrix}\psi_a(x)\\ &= \left(\frac{\boldsymbol{\sigma}\cdot\mathbf{p}}{2m}\varphi_a(x)\right)^*\sigma_i\varphi_a(x)\\ &\quad +\varphi_a^*(x)\sigma_\mu\frac{\boldsymbol{\sigma}\cdot\mathbf{p}}{2m}\varphi_a(x),\end{aligned} \tag{2.9}$$

which can be neglected due to the $\alpha^2 p/m$ terms. The only surviving terms, by hadronic current considerations only, are then the $\mu = 0$ part of the A^e-V^h interaction and $\mu = 1, 2, 3$ parts of the V^e-A^h interaction.

Electrons, on the other hand, are not well-described by a non-relativistic treatment, and thus relativistic operators should not be discarded. Further simplification is the omission of nuclear wave functions and their replacement with a predefined nuclear density $\rho(x) = \psi(x)^\dagger\psi(x)$. The final form of a hybrid non-relativistic-nucleon—relativistic-electron Hamiltonian is

$$\begin{aligned}H^{\mathrm{PV}} = &-\frac{G_F}{4\sqrt{2}}\left[(1-2\sin^2\theta_W)t_3 - 2\sin^2\theta_W\right]\gamma_5\rho(x)\\ &+\sum_{\mu=1}^{3}\frac{G_F}{4\sqrt{2}}(1-4\sin^2\theta_W)t_3\gamma_0\gamma_\mu\rho(x)\sigma_\mu,\end{aligned} \tag{2.10}$$

where the γ matrices operate on the electronic state, σ describes the spin of a nucleon, and t_3 is the eigenvalue of the isospin operator. The nuclear density can be taken to be, for example, a homogeneous Gaussian type function with an experimentally determined width. On the other hand, the size of a nucleus is minuscule as compared to other dimensions of an atom or a molecule, and thus it can be also approximated by a delta-function distribution. Nuclear density approximations in the PV context are investigated in Paper II and are discussed in Chapter 4.

The transition from one nucleon to the whole nucleus is not straightforward. The first part of the Hamiltonian (2.10), which contains no references to nucleon spins, can be generalized to the multi-nucleon case by simply summing over the contributions of individual nucleons. The second part contains an explicit reference to the nucleon spin. For the purposes of atomic

and molecular physics, the spin of the whole nucleus is more important than the spins of individual nucleons. Depending on the nuclear model used, the nucleon-spin-dependent part can be extrapolated as [45]

$$-\frac{G_F}{\sqrt{2}}K_n\frac{\kappa-1/2}{I(I+1)}\sum_{\mu=1}^{3}\gamma_0\gamma_\mu I_\mu\rho(x), \tag{2.11}$$

where κ is the Dirac angular quantum number. The total nuclear spin is represented by I and K_n is a factor depending on the nucleus. For example, constants for ^{133}Cs are $\kappa=4$, $I=7/2$ and $K\approx 0.05$.

The Hamiltonian (2.11) is not the only nuclear-spin-dependent parity-violating interaction at this level. Parity-violating radiative corrections to the interactions inside the nucleus give rise to the anapole moment of a nucleus (see, e.g., Ref. [32]). The effective anapole moment has the same structure as the nuclear-spin-dependent Z^0 direct exchange term (2.11) but with a different prefactor, and it has been measured only for the ^{133}Cs nucleus [31]. A curious fact about the anapole moment is that although it is supposed to be a radiative correction, it will dominate the interaction over the Z^0 exchange in heavy elements, e.g., in ^{133}Cs by almost 10 to 1 [32]. The anapole moment and the nuclear spin dependent Z^0 exchange term (2.11) are usually grouped together into a coefficient $K_N = K_a - (\kappa-1/2)/\kappa K_n$, where K_a refers to the anapole moment coefficient of the nucleus N.

The whole parity-violating Hamiltonian, including the anapole moment, can then be written as

$$H_I^{\mathrm{PV}} = \frac{G_F}{2\sqrt{2}}\sum_{N,i}Q_{W,N}\gamma_{5,i}\delta(\mathbf{r}_{iN}) + \frac{G_F}{\sqrt{2}}\sum_{N,i}\frac{K_N}{I_N(I_N+1)}\alpha_i\cdot\mathbf{I}_N\delta(\mathbf{r}_{iN}), \tag{2.12}$$

where the weak charge of nucleus N is $Q_{W,N}=(1-4\sin^2\theta_W)Z-N$ and $\alpha_i=\gamma_0\gamma_i$. If we take the value $\sin^2\theta_W=0.2312$ then the Q_W for the ^{133}Cs nucleus is -73.86. We can compare this to the value $Q_W(^{133}\mathrm{Cs})=-73.10\pm0.03$ [29] in which higher-order corrections to the interaction have been taken into account, and we can see that our value is within one per cent accuracy as we noted earlier. For lighter elements, a four-component relativistic treatment of the Hamiltonian (2.12) might therefore be unnecessary.

2.4 Two-component parity-violating Hamiltonian

Relativistic calculations are more expensive than non-relativistic for a couple of reasons. First, one has to include a basis set for the small component part of the wave function. An adequate basis set for the whole wave function turns out to be much larger than for the large components alone. Thus, with the formal $O(N^4)$ computation time scaling with respect to the basis set size N relativistic calculations can easily be more than an order of magnitude slower than non-relativistic calculations. Due to this practical constraint, we shall now examine an approximate two-component reduction of the full four-component operator using the Foldy–Wouthuysen (FW) transformation [46, 47].

The idea behind the FW and other similar transformations is to reduce the Dirac operator to a block-diagonal-dominant form,

$$H^D = \begin{pmatrix} h_{LL} & O(\alpha^n) \\ O(\alpha^n) & h_{SS} \end{pmatrix}, \tag{2.13}$$

using a unitary transformation that leaves the energy spectrum intact. If we are satisfied with a Hamiltonian that is correct to some order in the fine structure constant α, we can omit small off-diagonal terms in Eq. (2.13), and thus obtain separated equations for the small and large components. It should also be noted that the free electron Dirac equation can be separated analytically using the FW transformation [47].

The unitary matrix used in the FW transformation can be parameterized as

$$U = \begin{pmatrix} \frac{1}{\sqrt{1+X^\dagger X}} & \frac{1}{\sqrt{1+X^\dagger X}} X^\dagger \\ -\frac{1}{\sqrt{1+X^\dagger X}} X & \frac{1}{\sqrt{1+X^\dagger X}} \end{pmatrix}, \tag{2.14}$$

where X is the relation between the large and small components of the Dirac equation. Taking into account the external potential V, the relation between the large u_L and the small u_S components becomes

$$u_L = \frac{1}{2\alpha^{-2} + E - V} \boldsymbol{\sigma} \cdot \mathbf{p} u_S, \tag{2.15}$$

and

$$X = (2\alpha^{-2} + E - V)^{-1} \boldsymbol{\sigma} \cdot \mathbf{p}. \tag{2.16}$$

The term X can be expanded in $(E-V)\alpha^2/2$, thus providing a systematic way to improve decoupling of large and small components.

A major problem with the FW transformation is that it generates problematic operators, for example, the well-known mass-velocity and Fermi-contact operators proportional to $\mathbf{p}^4$ and $\delta(\mathbf{r}_K)$, respectively. Such operators are not bound from below and lead to a variational collapse of the wave function if they are used in a variational calculation. Instead of fully variational computations, operators generated by the FW method can be used as first-order perturbations to the non-relativistic Hamiltonian. Another serious drawback of the FW method is its convergence. Expansion in $(E-V)\alpha/2$ is troublesome if the potential has $1/r$ form, because there always exists areas near nuclei, where $(E-V) \gtrsim 2\alpha^{-2}$. Despite its problems, the FW transformation produces operators that are simple and relatively easy to implement, and thus enables its use for light elements, where perturbational treatment of relativity is sufficient, and for exploratory calculations on heavier elements, where quantitative accuracy is not crucial.

The actual procedure of using the FW transformation to obtain transformed one-electron parity-violating operators from the Hamiltonian in Eq. (2.12) is a somewhat laborious and error prone task and not shown here. The result be can divided into three parts (see Paper I),

$$\mathrm{H}^{\mathrm{PV}} = \mathrm{H}^{\mathrm{PV}(1)} + \mathrm{H}^{\mathrm{PV}(2)} + \mathrm{H}^{\mathrm{PV}(3)}, \tag{2.17}$$

in which

$$\mathrm{H}^{\mathrm{PV}(1)} = \frac{G_F\alpha}{2\sqrt{2}} \sum_N Q_{W,N} \sum_i \mathbf{s}_i \cdot [\mathbf{p}_i, \delta(\mathbf{r}_{iN})]_+ \tag{2.18}$$

$$\mathrm{H}^{\mathrm{PV}(2)} = -\frac{G_F\alpha}{2\sqrt{2}} \sum_N \lambda_N (1-4\sin^2\theta_W) \mathbf{I}_N \cdot \sum_i [\mathbf{p}_i, \delta(\mathbf{r}_{iN})]_+ \tag{2.19}$$

$$\mathrm{H}^{\mathrm{PV}(3)} = \mathrm{i}\frac{G_F\alpha}{2\sqrt{2}} \sum_N \lambda_N (1-4\sin^2\theta_W) \sum_i (\mathbf{s}_i \times \mathbf{I}_N) \cdot [\mathbf{p}_i, \delta(\mathbf{r}_{iN})]_- . \tag{2.20}$$

Here, i refers to electrons and s_i is the spin of the electron i, and commutators and anti-commutators are defined as

$$[A,B]_+ = AB + BA \;\; ; \;\; [A,B]_- = AB - BA. \tag{2.21}$$

We have also grouped the nucleus dependent factors of Eq. (2.12) into the constants λ_N.

The effects of external magnetic fields on the electrons can be included by making the minimal substitution

$$\mathbf{p}_i \rightarrow \mathbf{p}_i + \mathbf{A}_{i0} + \sum_K \mathbf{A}_{iK}, \tag{2.22}$$

where the contribution from the homogeneous external magnetic field $\mathbf{B}_0$ with respect to the gauge origin 0 is

$$\mathbf{A}_{i0} = \frac{1}{2}\mathbf{B}_0 \times \mathbf{r}_{i0}. \tag{2.23}$$

The magnetic vector potential generated by the nucleus K at the location of electron i is

$$\mathbf{A}_{iK} = \alpha^2 \gamma_K \mathbf{I}_K \times \frac{\mathbf{r}_{iK}}{r_{iK}^3}, \tag{2.24}$$

where γ_K is the gyromagnetic ratio of nucleus K. By making these substitutions to $\mathrm{H}^{\mathrm{PV}(1)}$, we obtain

$$\begin{aligned}
\mathrm{H}^{\mathrm{PV}(1)} &= h^{\mathrm{PV}(1)} + \mathrm{H}_{B_0}^{\mathrm{PV}(1)} + \sum_K \mathrm{H}_K^{\mathrm{PV}(1)} \\
h^{\mathrm{PV}(1)} &= \frac{G_F \alpha}{2\sqrt{2}} \sum_N Q_{W,N} \sum_i \mathbf{s}_i \cdot [-i\nabla_i, \delta(\mathbf{r}_{iN})]_+ \qquad (2.25) \\
\mathrm{H}_{B_0}^{\mathrm{PV}(1)} &= \sum_{\alpha\beta\gamma} \varepsilon_{\alpha\beta\gamma} \mathrm{B}_{0,\alpha} h_{B_0,\beta\gamma}^{\mathrm{PV}(1)} \ ; \\
h_{B_0,\beta\gamma}^{\mathrm{PV}(1)} &= \frac{G_F \alpha}{2\sqrt{2}} \sum_N Q_{W,N} \sum_i r_{i0,\beta} s_{i,\gamma} \delta(\mathbf{r}_{iN}) \qquad (2.26) \\
\mathrm{H}_K^{\mathrm{PV}(1)} &= \sum_{\alpha\beta\gamma} \varepsilon_{\alpha\beta\gamma} \mathrm{I}_{K,\alpha} h_{K,\beta\gamma}^{\mathrm{PV}(1)} \ ; \\
h_{K,\beta\gamma}^{\mathrm{PV}(1)} &= \frac{G_F \alpha^3}{\sqrt{2}} \gamma_K \sum_N Q_{W,N} \sum_i \frac{r_{iK,\beta}}{r_{iK}^3} \delta(\mathbf{r}_{iN}) s_{i,\gamma}. \qquad (2.27)
\end{aligned}$$

Here, we use Greek letters $\alpha,\beta,\gamma,\ldots$ to denote Cartesian indices. These should not be confused with the fine structure constant α. The Levi–Civita symbol $\varepsilon_{\alpha\beta\gamma}$ gives $+1$ for all symmetric permutations of $\alpha\beta\gamma$, -1 for anti-symmetric

permutations and 0 for other combinations. Similarly for $\mathrm{H}^{\mathrm{PV}(2)}$ we get

$$\begin{aligned}
\mathrm{H}^{\mathrm{PV}(2)} &= \sum_K \left[\mathrm{H}_K^{\mathrm{PV}(2)} + \mathrm{H}_{KB_0}^{\mathrm{PV}(2)} + \sum_L \mathrm{H}_{KL}^{\mathrm{PV}(2)} \right] \\
\mathrm{H}_K^{\mathrm{PV}(2)} &= \sum_\alpha h_{K,\alpha}^{\mathrm{PV}(2)} \mathrm{I}_{K,\alpha} \ ; \\
& \qquad h_{K,\alpha}^{\mathrm{PV}(2)} = -\frac{G_F \alpha}{2\sqrt{2}} \lambda_K (1 - 4\sin^2\theta_W) \sum_i [-i\nabla_{i,\alpha}, \delta(\mathbf{r}_{iK})]_+ \qquad (2.28) \\
\mathrm{H}_{KB_0}^{\mathrm{PV}(2)} &= \sum_{\alpha\beta\gamma} \varepsilon_{\alpha\beta\gamma} \mathrm{I}_{K,\alpha} \mathrm{B}_{0,\beta} h_{KB_0,\gamma}^{\mathrm{PV}(2)} \ ; \\
& \qquad h_{KB_0,\gamma}^{\mathrm{PV}(2)} = -\frac{G_F \alpha}{2\sqrt{2}} \lambda_K (1 - 4\sin^2\theta_W) \sum_i r_{iO,\gamma} \delta(\mathbf{r}_{iK}) \qquad (2.29) \\
\mathrm{H}_{KL}^{\mathrm{PV}(2)} &= \sum_{\alpha\beta\gamma} \varepsilon_{\alpha\beta\gamma} \mathrm{I}_{K,\alpha} \mathrm{I}_{L,\beta} h_{KL,\gamma}^{\mathrm{PV}(2)} \ ; \\
& \qquad h_{KL,\gamma}^{\mathrm{PV}(2)} = -\frac{G_F \alpha^3}{\sqrt{2}} (1 - 4\sin^2\theta_W) \times \\
& \qquad \left[\gamma_L \lambda_K \sum_i \frac{r_{iL,\gamma}}{r_{iL}^3} \delta(\mathbf{r}_{iK}) - \gamma_K \lambda_L \sum_i \frac{r_{iK,\gamma}}{r_{iK}^3} \delta(\mathbf{r}_{iL}) \right], \qquad (2.30)
\end{aligned}$$

and finally for $\mathrm{H}^{\mathrm{PV}(3)}$ there is only one term,

$$\begin{aligned}
\mathrm{H}_K^{\mathrm{PV}(3)} &= \sum_{\alpha\beta\gamma} \varepsilon_{\alpha\beta\gamma} h_{K,\alpha\beta}^{\mathrm{PV}(3)} \mathrm{I}_{K,\gamma} \ ; \qquad (2.31) \\
& \qquad h_{K,\alpha\beta}^{\mathrm{PV}(3)} = \mathrm{i} \frac{G_F \alpha}{\sqrt{2}} \lambda_K (1 - 4\sin^2\theta_W) \sum_i s_{i,\beta} [-i\nabla_{i,\alpha}, \delta(\mathbf{r}_{iK})]_- .
\end{aligned}$$

This term arises because there is a commutator in Eq. (2.20) instead of an anti-commutator as in the two other Hamiltonians.

3 Methods of quantum chemistry

To actually evaluate the parity-violating contributions to molecular properties, one needs to solve the many-body Schrödinger equation. A solution for both electronic and nuclear degrees of freedom simultaneously is a daunting task. To evade this problem, the Born–Oppenheimer (BO) approximation is introduced, where electrons are assumed to move much faster than nuclei and adapt to nuclear positions instantaneously. This is not a far fetched approximation, since nuclei are thousands of times heavier than electrons (and thus much slower). After the BO approximation is established, the problem of obtaining the electronic structure remains, and several further approximations are needed.

First, we have to overcome problems related to basis functions. In the case of the analytical solution of the hydrogen atom, the basis functions are combinations of generalized Laguerre polynomials and spherical harmonics. While an infinite number of those functions form a complete set, infinities are not suited for computers and we are forced to work with a finite subset of functions. One also has to consider the flexibility of the basis set. Most of the quantum chemistry programs use a combination of Gaussian and spherical-harmonic basis functions centered around the nuclei of a molecule.

After a finite one-electron basis set has been chosen, the Schrödinger equation for electrons has to be solved. Solving the equation precisely (in a given basis set) is limited to only the smallest of molecules. Computational effort for the precises solution scales exponentially with respect to the system size, and the current frontier using a moderately large basis set is around the C_2 molecule [48]. Several approximations have been developed, the simplest being Hartree–Fock (HF) theory, in which the electrons move in a mean-field generated by the other electrons of the system (and nuclei). There are sev-

eral ways to go beyond the HF theory, and the most common single-reference methods are configuration interaction (CI) and coupled cluster (CC) methods (see, e.g., Ref. [49] for multi-reference methods etc.). Both of them provide a systematic way to converge towards the exact solution. HF, CI and CC methods are usually referred to as wave function methods, because the whole wave function of the system can be obtained. Different approaches can also be taken: It turns out that the one-electron density is, in principle, enough to characterize the ground state of a system. Again, the exact solution of the ground state density requires specific knowledge, which is not available. Methods based on this principle are useful and grouped under the name density functional theory (DFT).

First, different methods for solving the electronic Schrödinger equation are discussed within the BO framework. A quick look at the the most common wave function methods (HF and CC) used in Papers I and II is provided. Then, the idea behind DFT is introduced alongside with a couple of common density functionals used in this thesis (Papers I–V). The electronic structure part is wrapped up by a glance at basis sets. Finally, methods to take into account vibrational corrections beyond the BO approximation using effective potential energy surfaces are described as used in Paper III.

3.1 Wave function methods

In this section, we shall introduce several wave function methods. With an emphasis on the molecules with a strong single-reference character, which includes the molecules used in Papers I-V, HF and CC methods are presented. We shall work in the second-quantization framework [50].

3.1.1 Hartree–Fock theory

The simplest wave function that we can construct in second quantization is one configuration. Not every configuration qualifies as a meaningful wave function, but we need to find the optimal one. We start by making an initial guess with a set of parameters, which can be used to variationally minimize the energy. One way to express a suitable trial configuration is via an expo-

nential parameterization

$$|\mathrm{HF}(\kappa)\rangle = \exp(\kappa)|0\rangle, \tag{3.1}$$

where

$$\kappa = \sum_{PQ} \kappa_{PQ} a_P^\dagger a_Q. \tag{3.2}$$

κ_{PQ} are the orbital rotation parameters, which should also be adapted to the spin or spatial symmetry of a system, e.g., we should get rid of rotations between singlet and triplet configurations in a closed-shell molecule. In second quantization, $a_P^\dagger$ and a_P are creation and annihilation operators for the state P (see Ref. [50] for details). If we require κ to be antisymmetric, the exponential in Eq. (3.1) will be an unitary operator transforming one configuration to another while conserving the normalization and inner products. Using this parameterization, we can write the optimal one-configuration energy as

$$E_{\mathrm{HF}} = \min_{\kappa} \langle \mathrm{HF}(\kappa)|H|\mathrm{HF}(\kappa)\rangle. \tag{3.3}$$

Variational minimization using only one configuration is called the Hartree–Fock approximation. Getting the actual HF energy is a matter of finding a suitable method to find the minimum in Eq. (3.3). One way to proceed is to further develop Eq. (3.3) to the traditional canonical form [50], or to obtain the optimal configuration by using modern density-based methods [50, 51].

HF theory works well for systems, in which a single configuration is dominant. The ground states of most closed-shell main-group molecules and open-shell molecules with simple electronic structure are such cases. Transition metals or molecules in stretched geometries usually require multiconfigurational methods. Nowadays, HF has been mostly superseded by more advanced WF and DFT methods, but is still used in conjunction and as a starting point for other methods, see Papers I and II.

3.1.2 Beyond Hartree–Fock

The simplest improvement over HF is to include more configurations in our trial wave function. If we include all of the configurations, we have an expan-

sion, which covers the whole parameter space and the solution in that space corresponds to the previously mentioned exact solution of the Schrödinger equation in the given basis. The inclusion of all possible determinants is often called full configuration interaction (FCI) or exact diagonalization.

The FCI solution is nearly always too expensive to obtain. A systematic way to approach the FCI limit is to generate single, double, triple etc. excitations from a reference configuration (often the HF state). For the configuration interaction (CI) method, a linear parameterization for excitations is used and equations are solved variationally. Thus, the CI wave function is

$$|\mathrm{CI}\rangle = (C_1 + C_2 + ...)\,|\mathrm{HF}\rangle = \left(\sum_{AI} C_A^I a_A^\dagger a_I + \sum_{AIBJ} C_{AB}^{IJ} a_I^\dagger a_J^\dagger a_A a_B + ...\right)|\mathrm{HF}\rangle, \tag{3.4}$$

where C_A^I and C_{AB}^{IJ} are coefficients for single and double excitations, respectively, up to some order (e.g., including only single and double excitations). The resulting equations for the C coefficients can be solved variationally. Truncated CI expansions are easy to calculate, but they suffer from the size-extensivity problem, i.e. the correlation energy of a system does not scale properly with respect to the number of non-interacting fragments. Size-extensivity of CI with single and double excitations can be established [52], but the result is not attractive in cost–accuracy ratio as compared to the corresponding coupled-cluster model.

Coupled cluster theory relies on an exponential parameterization

$$|\mathrm{CC}\rangle = \exp(T)|\mathrm{HF}\rangle, \tag{3.5}$$

where the cluster operator is

$$T = T_1 + T_2 + ... = \sum_{AI} t_A^I a_A^\dagger a_I + \sum_{AIBJ} t_{AB}^{IJ} a_I^\dagger a_J^\dagger a_A a_B + ... \tag{3.6}$$

T_1 and T_2 are single and double excitation operators, respectively, with excitation amplitude parameters t_A^I and t_{AB}^{IJ}. The exponential of an operator is defined through its Taylor expansion.

Exponential parameterization has a couple of compelling features when using truncated expansions. If the CC equation (3.5) would be expanded and

compared to the CI wave function (3.4), the fact that low-order CC excitations would be present in some form in all higher-order CI excitations would emerge (see Ref. [50]). This means that truncated CC expansions provide a more compact representation of the wave function than the corresponding CI expansion. For example, CISD and CCSD wave functions have the same number of parameters, but CCSD provides much better energies and properties in most cases. Due to the exponential parameterization, the CC method is also size-extensive when using truncated expansions.

The variational form of the CC equations,

$$\mathrm{E_{CC}} = \frac{\langle \mathrm{CC}|H|\mathrm{CC}\rangle}{\langle \mathrm{CC}|\mathrm{CC}\rangle}, \tag{3.7}$$

is troublesome, because exponentials in Eq. (3.7) do not terminate until the whole excitation space is covered. In practice, this leads to a computational cost similar to FCI, even for a truncated expansion of the T operator, and thus all the CC calculations are done non-variationally. The non-variational nature of CC calculations has its drawbacks, but with an adequate basis sets, truncated CC expansions provide good results.

Over the years, numerous approximate CC models have been developed. The current hierarchy in increasing accuracy for closed shell molecules goes like HF, CC2, CCSD, CCSD(T), CC3, CCSDT, CCSDT(Q), and so forth. In general, CCSD(T)/CC3 is considered to be very close to chemical accuracy in energy-based properties (e.g., vibrational frequencies), although higher-order excitations are sometimes needed even up to the connected quadruple excitations [53, 54]. In this thesis, we have used the beginning of the CC series, namely HF, CC2 and CCSD methods, to examine electron correlation effects to the PV properties in Paper II. Some of the result show large discrepancies between CC2 and CCSD results, and thus it would be necessary (although not practical) to include also CC3 and perhaps CCSDT results for very high accuracy.

3.2 Density functional theory

3.2.1 Principles

The Foundation of modern DFT rests on two theorems by Hohenberg and Kohn [55]. The first one establishes an one-to-one correspondence between the exact many-body ground-state wave function and the corresponding one-electron density. The other theorem states that the one-electron density corresponding to a ground-state wave function is variational, a property which can be used to optimize the density without any references to wave functions. Using the density ρ as a basic variable, the ground state energy can be written in a functional form as

$$E[\rho] = T[\rho] + V_{ee}[\rho] + \int \rho(\mathbf{r}) v(\mathbf{r}) d\mathbf{r}, \tag{3.8}$$

where $T[\rho]$ and $V_{ee}[\rho]$ are the kinetic energy and electron-electron repulsion terms, respectively. The last term is the effect of an external potential $v(\mathbf{r})$, which in a molecular case (in the BO approximation) is the potential generated by nuclear charges. Functionals $T[\rho]$ and $V_{ee}[\rho]$ are independent on the system (as the $v(\mathbf{r})$ specifies the configuration of the system, excluding the number of electrons), but unfortunately, their exact forms are unknown. This is the main (and to some extent only) obstacle faced by DFT.

A useful approximation to Eq. (3.8) was made by Kohn and Sham [56]: As a starting point, they separated out the kinetic energy of a non-interacting system of density ρ,

$$T_n[\rho] = -\frac{1}{2} \sum_i \int \varphi_i^*(\mathbf{r}) \nabla_i^2 \varphi_i(\mathbf{r}) d\mathbf{r}, \tag{3.9}$$

where orbitals φ_i form the density

$$\rho(\mathbf{r}) = \sum_i |\varphi_i(\mathbf{r})|^2. \tag{3.10}$$

By Using these, Eq. (3.8) can be used to derive variational equations for orbitals φ_i, and the end result is similar to self-consistent field equations (SCF)

of the HF theory,

$$\left[-\frac{1}{2}\nabla^2 + v_{eff}(\mathbf{r})\right]\varphi_i(\mathbf{r}) = \varepsilon_i\varphi_i(\mathbf{r}). \tag{3.11}$$

Here, we have grouped several terms into an effective potential

$$v_{eff}(\mathbf{r}) = v(\mathbf{r}) + \int \frac{\rho(\mathbf{r}')}{|\mathbf{r}-\mathbf{r}'|}d\mathbf{r}' + \frac{\partial E_{\mathrm{XC}}[\rho]}{\partial\rho}, \tag{3.12}$$

where the last term is the functional derivative of a so-called exchange-correlation (XC) term

$$E_{\mathrm{XC}}[\rho] = T[\rho] - T_n[\rho] + V_{ee}[\rho] - \int \frac{\rho(\mathbf{r})\rho(\mathbf{r}')}{|\mathbf{r}-\mathbf{r}'|}d\mathbf{r}d\mathbf{r}'. \tag{3.13}$$

In other words, the XC functional E_{XC} includes all the correlation and Fermi exchange effects of a system. Depending on the exact form of the E_{XC}, the SCF equations of (3.11) can be cheaper, equal to, or more expensive to evaluate than the corresponding HF SCF equations. Assuming that the Hohenberg–Kohn theorems are valid for approximate E_{XC}, the road for different approximate approaches is open.

3.2.2 Functionals

Here we will give descriptions of XC functionals used in this thesis. Numerous other functionals have been developed with or without empirical parameter fitting, but the general approach is to construct functionals to agree with some limiting cases. For example, most of the functionals used in solid state physics are developed in such fashion that they will conform to the free electron gas limit, when no external potential is present. Also, often the exchange and correlation parts of the XC function are separated,

$$E_{\mathrm{XC}}[\rho] = E_{\mathrm{X}}[\rho] + E_{\mathrm{C}}[\rho]. \tag{3.14}$$

Systematic construction of better functionals in DFT is limited, but some groups (“rungs”) of better or worse performing functionals can be defined [57].

Local density approximation

The local density approximation (LDA), as the name already suggests, assumes that the XC functional depends only on the density at a given point, but not on its derivatives, for example. This is a good assumption for systems with a slowly varying electron density. One such system is the uniform electron gas, where the exchange functional is known analytically (commonly known as the Dirac exchange) [58]. As a curious side note, this was the functional that Slater used in a scaled form as a cheap approximation for the HF theory [59]. The correlation part of the uniform electron gas is not known analytically, but based on the accurate quantum Monte Carlo simulations of Ceperley and Alder [60], Vosko, Wilk and Nusair used these to fit a local density functional for the correlation part [61]. LDA, which is commonly used as a synonym for $E_{\mathrm{X}}^{\mathrm{Dirac}} + E_{\mathrm{C}}^{\mathrm{VWN}}$, has not been proved to be very useful for molecules, but it is included in many other functionals.

Generalized gradient approximation

The generalized gradient approximation (GGA) is used to improve upon LDA by including gradient terms in both the exchange and correlation parts of the XC functional. Several different types of GGAs exist and we will only give some background information about functionals used in this thesis.

One of the successful GGA correlation functionals was developed by Perdew [62]. He constructed his functional to satisfy some physical conditions of the inhomogeneous electron gas for slowly varying density based on the earlier work of Langreth and Mehl (LM) [63] and added his own modifications. The functional includes one free parameter, which has been chosen to fit the correlation energy of the neon atom. The functional, named P86, was a significant improvement over the LDA and LM functionals, and has been used in various contexts ever since.

For the exchange part, a widely used functional is Becke's functional from 1988, called as B88 [64]. A simple gradient correction to the LDA exchange functional leads to an asymptotically diverging exchange potential for finite systems, which is clearly awkward. Becke introduced a semi-empirical cor-

rection to the gradient term with one parameter, which was fitted to HF exchange energies of noble gas atoms from helium to radon. B88 exchange has been combined with many correlation functionals. For example, a combination of B88 and P86, the BP86 functional, has been used in this thesis to calculate PV properties in Papers II and V.

Another widely-used correlation functional is the one by Lee, Yang and Parr (LYP) [65]. They constructed their functional using a somewhat different route than Perdew. The LYP functional is based on the approximate method of calculating the correlation energy from the second-order HF density matrix by Colle and Salvetti [66]. The Colle–Salvetti (CS) method includes four parameters, which are determined using the helium atom, and it provides reasonable correlation energies for light elements [66]. The LYP functional has been successfully used in variety of chemical systems. Its combination with the B88 functional, BLYP, is used in Paper I.

All of the functionals mentioned above include some parameters that have been fitted to a very small set of atomic data. Nowadays, the emphasis is on more general functionals, which do not depend on fitting parameters, but rely on implementing a set of suitable analytical conditions instead (for a short list, see Ref. [57]). One of the first such functionals was the Perdew–Burke–Ernzerhof (PBE) functional. It satisfies many asymptotic properties and scaling laws of the (slowly varying) inhomogeneous electron gas, and is formulated in such way that its parameters are determined by analytical conditions. Although PBE is free of parameters, its performance is usually similar to other GGA functionals, as can be seen in Paper II, where it has been compared to the BP86 functional. Similar to PBE in spirit is the Perdew–Wang 1991 (PW91) functional [67], which was constructed as an analytical fit to a first-principles numerical functional. Both functionals produce essentially the same results [68], but the simpler form of the PBE functional makes it a more compelling choice. Nevertheless, PW91 is used in Paper V to provide an alternative functional formulation to BP86.

Hybrid functionals

The HF theory has a well defined exchange part. Inclusion of the HF (or exact) exchange term into DFT improved the accuracy of DFT significantly

in molecular calculations. Perhaps the most well-known "hybrid" functional is the B3LYP functional [69, 70] that combines different exchange and correlation functionals with HF exchange,

$$E_{\mathrm{XC}}^{\mathrm{B3LYP}} = (1-a_0)E_{\mathrm{X}}^{\mathrm{LDA}} + a_0 E_{\mathrm{X}}^{\mathrm{HF}} + a_{\mathrm{X}} E^{\mathrm{B88}} + a_{\mathrm{C}} E_{\mathrm{C}}^{\mathrm{LYP}} + (1-a_{\mathrm{C}})E_{\mathrm{C}}^{\mathrm{VWN}}, \tag{3.15}$$

where $a_0 = 0.2$, $a_{\mathrm{X}} = 0.72$ and $a_{\mathrm{C}} = 0.81$ are parameters that are fitted to reproduce heats of formations of a set of small molecules [69]. The B3LYP functional has been successful in various chemical applications and it can even rival some of the correlated WF methods. It has also been used in Papers I-V as a correlated method of choice. In Paper II, it was shown to reproduce electron correlation effects at least qualitatively when compared to CCSD. Similar "hybridization" has been done for the PBE functional [71], too, but with a single mixing parameter for the exact exchange,

$$E_{\mathrm{XC}}^{\mathrm{PBE0}} = (1-b_{\mathrm{X}})E_{\mathrm{X}}^{\mathrm{PBE}} + b_{\mathrm{X}} E_{\mathrm{X}}^{\mathrm{HF}} + E_{\mathrm{C}}^{\mathrm{PBE}}. \tag{3.16}$$

Based on the lowest-order perturbation theory arguments, Perdew, Ernzerhof and Burke provided rationale for the approximate value $b_{\mathrm{X}} = 0.25$ [72], and indeed, the PBE0 functional is most of the time equal or slightly better than the B3LYP functional in terms of predictive power in chemical applications, also in PV properties as seen in Paper II.

3.3 Basis sets

As noted before, the Schrödinger equation is solved using an expansion in a finite one-particle basis set, but the choice of a suitable basis set is not a simple matter. Naturally, one wants the basis set to be as close to completeness as possible and still be compact so that the number of free parameters in electronic structure calculations would not increase beyond what is possible. Due to the second "wish", the first one is usually partially discarded and a basis set, which is believed to give a reasonable description of the situation, is chosen.

Modern basis sets used in most of the quantum chemical calculations are based on combinations of Gaussian type functions and real solid harmonic

functions that are closely related to more familiar spherical harmonic functions. The form of a Gaussian type orbital (GTO) is

$$\chi^{\mathrm{GTO}}_{\alpha_{nl}lm} = N^{\mathrm{GTO}}_{\alpha_{nl}lm} S_{lm} \exp(-\alpha_{nl} r^2), \tag{3.17}$$

where n, l and m are indices that are closely related to the quantum numbers of the hydrogen atom, namely the principal, angular momentum and magnetic quantum numbers, respectively. $N^{\mathrm{GTO}}_{\alpha_{nl}lm}$ is the normalization constant and S_{lm} is a regular solid harmonic function. Coefficients α_{nl} are usually determined so that a linear combination of GTOs resembles some specific atomic orbital. For a fixed l, it is possible to systematically vary coefficients α_{nl} so that a set of such GTOs forms a complete set [73]. Other bases are also in use, for example, Slater type orbitals (STO), in which the dominant term at large distances is proportional to $\exp(-\alpha_{nl} r)$ and the r-dependence is also different near nucleus. Unlike STOs, GTOs do not describe the so-called nuclear cusp condition correctly, but integrals over GTOs can be evaluated analytically and faster than over STOs. The ease of evaluation of GTOs usually outweighs the requirement of more functions to satisfy the nuclear cusp condition, and thus GTOs are more common than STOs nowadays.

Construction of a compact but accurate set of α_{nl} coefficients for different l-values is difficult for a general case. Usually, a set of α_{nl} coefficients is constructed in such manner that the total energy of a certain individual atom is minimized up to the maximum value of l occupied if the electrons of the atom would be arranged into eigenstates of the hydrogen atom. These atom-specific basis sets can then be used as such for calculations with molecules, but usually they are augmented to at least allow for the polarization of the charge density due to other atoms. In the first-order approximation, polarization increases the maximum angular quantum number of a basis set by one. New α_{nl} coefficients cannot be optimized using individual atoms only, but the coefficients are optimized using a small set of test molecules. Different basis sets also differ by how much flexibility is assigned to different regions of space and quantum numbers. Core orbitals are not much affected by the external environment and linear combinations of functions are grouped together, that is, contracted. In this way the number of free parameters in a basis set can be kept low. Valence orbitals are usually left uncontracted and

often basis sets are augmented with diffuse valence functions to cover the space between atoms in molecules. For correlated calculations, the Coulomb hole introduces an extra difficulty that requires high angular momentum basis functions.

Many different basis-set families have been developed over the years. For correlated calculations, the contemporary standard set is Dunning's polarized correlation consistent basis sets, which are constructed to systematically increase the quality of the description of the Coulomb hole. Those sets are also used in this thesis in Papers II and III to provide systematic increase in quality for CC2 and CCSD methods. The basic sets are labelled cc-pVXZ (X = D, T, Z, Q,...) [74, 75], in which each core orbital is described by one contracted GTO and the valence orbitals are described by X GTOs with an emphasis on the systematic improvement of the core-valence correlation energy. These sets can be augmented by adding diffuse functions for the valence region (aug-cc-pVXZ) [74–76] or by adding more flexibility to the core region (cc-pwCVXZ) [77].

In addition to the ground state energy (with or without correlation), basis sets can also be optimized for molecular properties. For example, a finite basis set introduces errors due to the incomplete gauge invariance of the electromagnetic interaction, i.e., expressions are dependent on the choice of the gauge origin. The IGLO basis sets were constructed from the Huzinaga primitive basis sets [78] and polarized and contracted by Kutzelnigg [79] to minimize the gauge origin error. The IGLO sets provide good energies and magnetic properties with reasonable computational cost and are used in Papers I, IV, and V. Special basis sets for many other properties have also been developed. Many other widely used basis-set families have also been developed, but are not mentioned here.

3.4 Vibrational corrections

The "balls and sticks" picture of molecules is somewhat spurious since it shows a molecule consisting of nuclei that are connected by rigid bonds. To some extent, this is how many quantum chemical calculations are done since the nuclear positions are usually held fixed (BO approximation). However,

the correct quantum mechanical description of a molecule requires a quantum mechanical treatment of nuclei in addition to electrons. Similarly to the zero-point vibrations of the quantum harmonic oscillator, the molecular ground state is also "vibrating" and energies and properties should be evaluated accordingly.

3.4.1 Vibrational Hamiltonian

Calculations without the BO approximation have been carried out by several groups (see, e.g., Refs. [80–83]), but all the common challenges of electronic structure calculations are even more pronouncedly present in nucleus-electron calculations. First, the choice of the Hamiltonian is a non-trivial task. Preferably, one uses a Hamiltonian that does not take into account rotational and translational motion of the whole molecule. Basis set problems are also present. Most of the calculations are made using Gaussian type orbitals for both electrons and nuclei. For many types of motions, such as large amplitude torsional motion, Gaussian orbitals placed in nuclear positions obtained from a BO geometry optimization are not sufficient, and the accuracy of distributed Gaussian orbitals is also questionable. Finally, the problem of correlation is escalated to include electron–nucleus and nucleus–nucleus cases, where the correlation can be very strong, in addition of the traditional electron–electron correlation. Most of the calculations use HF, CI, CC, perturbation theory and multi-configurational methods. Nuclear DFT has been also developed, but currently functionals are of the X_α (originally developed as a cheap alternative to HF) quality [80]. These methods can provide interesting new views on dynamics of molecules, provided that problems with basis sets and correlation can be treated.

The situation improves notably, if approximations are allowed. The first is the Born–Oppenheimer approximation mentioned earlier, where electronic and nuclear degrees of freedom are separated from each other in such way that electrons see a rigid nuclear frame in which they can adapt and nuclei move on a BO potential energy surface (PES) generated by electrons. This simplifies greatly the electronic part, and in principle, also the nuclear part. More complications for the nuclear part arise from the separation of the exter-

nal motion from the internal, translation of the center of mass and rotation of the whole molecule from internal vibrations between the nuclei. Separation of external and internal motion can be done (approximately) by imposing the Eckart conditions [84] on the Hamiltonian. The result is a rather uninviting form of the vibrational Hamiltonian [85],

$$H(\mathbf{Q}) = -\frac{1}{2}\sum_{k=1}^{3N-6}\frac{\partial^2}{\partial Q_k^2} + \frac{1}{2}\sum_{\alpha\beta\in\{x,y,z\}}(J_\alpha - \pi_\alpha)\mu_{\alpha\beta}(J_\beta - \pi_\beta) - \frac{1}{8}\sum_{\alpha\in\{x,y,z\}}\mu_{\alpha\alpha} + V(\mathbf{Q}), \tag{3.18}$$

using the normal coordinates Q_k. Normal coordinates are delocal, i.e., they consist of simultaneous in-phase motions of several nuclei, and they do not include external translational or rotational degrees of freedom, hence $3N-6$ in summations (for non-linear molecules). Rotation of the whole nuclear system is still present in the Hamiltonian in the form of the total angular momentum operator $\mathbf{J}$. Of the other terms, π is the vibrational angular momentum, and μ is the effective reciprocal inertia tensor. For more information on this subject, see, e.g., Ref. [86]. In general, the Hamiltonian of Eq. (3.18) is unnecessarily complicated for most cases, and angular momentum terms are usually omitted so that the simplified Hamiltonian is

$$H(\mathbf{Q}) = -\frac{1}{2}\sum_k\frac{\partial^2}{\partial Q_k^2} + V(\mathbf{Q}). \tag{3.19}$$

While the kinetic energy part of the Hamiltonian is resolved using approximations described above (which might not be suitable in every case), an efficient description of the potential $V(\mathbf{Q})$ is developed next.

3.4.2 Generation of a potential energy surface

The simplest way to form the potential is to use the harmonic approximation for nuclear potentials. In this approximation, the potential is expanded on a series that is truncated after quadratic terms. In addition, nuclei are initially thought to be in their equilibrium positions, which means that the first deriva-

tives of the potential are zero. The result is

$$V(\mathbf{x}) = \frac{1}{2}\sum_{ij}\frac{\partial^2 V}{\partial x_i \partial x_j}x_i x_j, \tag{3.20}$$

where the x_i refer to Cartesian coordinates of the nuclei. This potential can then be combined with the kinetic energy term (in Cartesian coordinates) and further diagonalized so that the potential (and also kinetic energy) is obtained in terms of normal coordinates,

$$V(\mathbf{Q}) = \sum_i f_{ii} Q_i^2. \tag{3.21}$$

Overall, this leads to harmonic oscillator type equations and is easily solved to obtain harmonic vibrational frequencies. Advantages of the harmonic potential are its simplicity and the fact that the second derivatives of the potential can be evaluated analytically in most quantum chemistry codes and for most of the methods available. As a "first" order approximation, in a sense, it provides good results for deep small amplitude potentials but fails with more shallow or wide potentials. A natural way of improvement is to take anharmonicity into account, i.e., the fact that the potential is not truly harmonic. This is done by expanding the potential to higher orders, and it is indeed the way to proceed. Higher-order derivatives are in practice evaluated by calculating several points near the equilibrium position and then calculating the derivatives numerically. If the expansion is made in a simple fashion, the number of single-point electronic structure calculations increases rapidly. From past experiences it has been found that the anharmonicity of the potential is more important than the couplings between different modes in the potential, e.g., terms like

$$V(\mathbf{Q}) = \sum_{ijk} f_{ijk} Q_i Q_j Q_k. \tag{3.22}$$

It is therefore more economical to use high-order Taylor expansions with only a limited number of mode couplings. For this purpose, we adopt mode-coupled potentials that are referred to as nMmT, where n is the number of modes coupled and m is the order of the Taylor expansion. In this language, the harmonic potential of Eq. (3.21) would be 1M2T, and the minimal poten-

tial containing the term in Eq. (3.22) would be 3M3T in turn. Actual generation of potentials of this type includes some technical details, such as overcounting and numerical integration, and a detailed description of the process is left to Ref. [87]. The Taylor expansions of the potential are, however, not without problems. First, it is known that the convergence of the Taylor expansion is not guaranteed and that can also be a problem in vibrational calculations. Another problem is that a truncated Taylor expansion is not necessarily bound from below [88]. In the near-equilibrium position, truncated expansions usually provide reliable potentials, but further away from the equilibrium the potential might collapse to minus infinity. If one uses a basis (see below) that also explores the outer limits of a potential, the unboundedness can lead to unstable results. To overcome these limitations, a grid-based method has been developed [89].

In the grid-based method, the same kind of restricted mode coupled potentials are used as in the perturbational method, but instead of polynomials the grid is represented by discrete points. The grid points are generated by defining a range in which the points can be located. One way to define the range is to take the turning points of a quantum harmonic oscillator,

$$x_{TP} = \sqrt{\frac{2\hbar}{\omega}\left(\nu + \frac{1}{2}\right)}, \tag{3.23}$$

where ω is the energy of the mode, and ν is the excitation level (in our case, it is chosen to be 10). A coarse, electronic-structure-calculation-based grid is further interpolated by splines to provide a smooth and more stable potential. In the multi-mode coupled case, all the combinations of grid points are evaluated. Different grids are denoted by $M_m N_n K_k$, where the capital letters present numbers of grid points in one, two and three mode coupled cases, respectively. Small letters are used to denote restrictions for the grid points near the equilibrium (see Ref. [89]). While being numerically more stable and treating anharmonicity, in principle exactly, the grids can be expensive to generate. The number of electronic structure calculations required is

$$N = \sum_{n=0}^{N} \binom{N}{n} (K_n)^n, \tag{3.24}$$

where n is the number of coupled modes with a maximum of N modes, and the standard definition of binomial coefficients is used. K_n is the number of grid points in the n mode coupled case. For example, with a $64_1 16_1 4_1$ grid, the number of points required is 5505, and increases in numbers of points in multi-mode coupled cases clearly increases the total number of calculations beyond reach.

The solution of the vibrational Hamiltonian can then proceed by expanding the Hamiltonian in a finite basis, much like in electronic structure calculations. A natural choice would be to use combinations of harmonic oscillator functions expressed as a function of normal coordinates, but one might use other functions like distributed Gaussians [90]. Second quantization also works for vibrational systems, but as the vibrational modes have a bosonic nature, one does not need to use the anti-symmetry condition of electrons, and thus a simple Hartree product will be sufficient for a configuration state. When the second quantization framework is established, it easy to formulate approximate solutions, such as vibrational self consistent field theory (VSCF), vibrational perturbation theory (VMP), vibrational configuration integration (VCI) and vibrational coupled cluster theory (VCC), with similar strengths and weaknesses as in their electronic structure counterparts. For a review of second quantization and methods, see Ref. [91].

4 Results of parity violation in molecular magnetic resonance properties

In this section, we will review the results of Papers I-V. First, we will introduce a convenient framework for molecular properties in terms of response functions, and subsequently write down the expressions for PV contributions to selected nuclear magnetic resonance (NMR) and electron spin resonance (ESR) spectral parameters. Then, we will examine the approximations made, namely the choice of the Hamiltonian, basis set and correlation models. Model systems for the NMR part are small dihedral molecules, H_2X_2, where X = ^{17}O, ^{33}S and ^{77}Se, and larger ^{13}CHF^{35}Cl^{79}Br and ^{13}CHF^{79}Br^{127}I molecules. Vibrational corrections to the PV shielding constant contributions are investigated using the ^{13}CHF^{35}Cl^{79}Br molecule. Molecules for PV g-tensor contributions calculations are CH_3XOH, where X = N, P, As, Sb, which have doublet electronic character, i.e., one unpaired electron.

4.1 Molecular magnetic resonance properties

Magnetic resonance properties of molecules are related to external magnetic fields used to probe them, as the name suggests. NMR and ESR spectroscopies have been used in many applications, e.g., magnetic resonance imaging, structure determination of proteins, etc. An external magnetic field is used to probe nuclear spins in NMR spectroscopy. Coupling strengths of the magnetic field and nuclear spins are affected by the surrounding elec-

tronic structure, which varies from molecule to molecule. Measured coupling strengths can then be used to obtain information about molecular environments of nuclei, or the other way around, to obtain information about nuclei, if the electronic structure is known (by accurate computations, for example). ESR spectroscopy works similarly, but the spins of unpaired electrons are used instead of nuclear spins. For details of definitions and computational aspects, see Ref. [92].

Spectroscopically measured quantities are conveniently expressed as derivatives of the molecular energy. For example, the molecular energy in the presence of the nuclear spin of nucleus K, $\mathbf{I}_K$, and an external magnetic field, $\mathbf{B}_0$, can be expanded as

$$\begin{aligned} E(\mathbf{I}_K,\mathbf{B}_0) = E_0 &+ \left.\frac{\partial E(\mathbf{I}_K,\mathbf{B}_0)}{\partial \mathbf{I}_K}\right|_{\mathbf{I}_K=\mathbf{0}} \mathbf{I}_K + \left.\frac{\partial E(\mathbf{I}_K,\mathbf{B}_0)}{\partial \mathbf{B}_0}\right|_{\mathbf{B}_0=\mathbf{0}} \mathbf{B}_0 + \\ &\frac{1}{2}\left.\frac{\partial^2 E(\mathbf{I}_K,\mathbf{B}_0)}{\partial \mathbf{I}_K \partial \mathbf{B}_0}\right|_{\mathbf{I}_K=\mathbf{0},\mathbf{B}_0=\mathbf{0}} \mathbf{I}_K\mathbf{B}_0 + \frac{1}{2}\left.\frac{\partial^2 E(\mathbf{I}_K,\mathbf{I}_K)}{\partial \mathbf{I}_K \partial \mathbf{I}_K}\right|_{\mathbf{I}_K=\mathbf{0}} \mathbf{I}_K\mathbf{I}_K + \\ &\frac{1}{2}\left.\frac{\partial^2 E(\mathbf{B}_0,\mathbf{B}_0)}{\partial \mathbf{B}_0 \partial \mathbf{B}_0}\right|_{\mathbf{B}_0=\mathbf{0}} \mathbf{B}_0\mathbf{B}_0 + \ldots \end{aligned} \tag{4.1}$$

The expression would continue with higher-order derivatives.

The leading-order property depending on the external magnetic field and the nuclear spin is the NMR shielding tensor. The shielding tensor of nucleus K can then be expressed as (ε and τ denote Cartesian indices),

$$\sigma_{K,\varepsilon\tau} = \frac{1}{\gamma_K}\left.\frac{\partial^2 E(\mathbf{I}_K,\mathbf{B}_0)}{\partial \mathrm{I}_{K,\varepsilon}\partial \mathrm{B}_{0,\tau}}\right|_{\mathbf{I}_K=\mathbf{0},\mathbf{B}_0=\mathbf{0}}. \tag{4.2}$$

Here, γ_K refers to the gyromagnetic ratio of the nucleus K and is included for convenience. If, for example, the external magnetic field is very strong, non-linear effects should also be considered in the total response of the energy to $\mathbf{I}_K$ and $\mathbf{B}_0$, but with tractable magnetic fields, non-linear effects are negligible [93].

The nuclear shielding tensor is not the only spectroscopic observable in NMR spectroscopy. Among others, there is the nuclear spin-spin coupling, which describes the coupling of nuclear spins through the electronic structure. The spin-spin coupling splits the NMR shielding resonance peaks into

multiples with line separations that are independent of the magnetic field used in the measurement. The expression for the spin-spin coupling in terms of energy derivatives is

$$J_{KL,\varepsilon\tau} = \frac{1}{2\pi} \left. \frac{\partial^2 E(\mathbf{I}_K, \mathbf{I}_L)}{\partial \mathrm{I}_{K,\varepsilon} \partial \mathrm{I}_{L,\tau}} \right|_{\mathbf{I}_K=\mathbf{0}, \mathbf{I}_L=\mathbf{0}}. \tag{4.3}$$

In ESR spectroscopy, the so called g-tensor measures the effects of the molecular environment on the free-electron $g_e \approx 2.0023$ value with the Hamiltonian

$$\mathrm{H} = \mu_B \mathbf{s} \cdot \mathbf{g} \cdot \mathbf{B}_0, \tag{4.4}$$

where the Bohr magneton $\mu_B = 1/2$. Differences to the free-electron g-tensor are formulated by separating it from the total g-tensor,

$$\mathbf{g} = g_e \mathbf{1} + \Delta\mathbf{g}. \tag{4.5}$$

Again, the g-shift tensor $\Delta\mathbf{g}$ can be expressed using the energy derivatives,

$$\Delta g_{\varepsilon\tau} = \frac{1}{\mu_B} \left. \frac{\partial^2 E(\mathbf{s}, \mathrm{B}_0)}{\partial s_\varepsilon \partial \mathrm{B}_{0,\tau}} \right|_{\mathbf{B}_0=\mathbf{0}, \mathbf{s}=\mathbf{0}} - g_e \delta_{\varepsilon\tau}. \tag{4.6}$$

With well-defined expressions for some of the molecular magnetic properties, we can proceed to find the parity-violating contributions to them.

4.2 Parity-violating contributions to molecular magnetic resonance properties

Using the parity-violating operators of Chapter 2 and those obtained in a similar way from the Dirac–Coulomb–Breit operator (see, e.g., Ref. [92]), we obtain parity-violating contributions to different properties using perturbation theory. For the sake of clarity, we shall use the notation of response theory, which will be introduced next. The time-dependent response of an expecta-

tion value of the operator A in the presence of a perturbation V is [94, 95]

$$A(t) = \langle 0|A|0\rangle + \int_{-\infty}^{\infty} d\omega_1 \exp[(-i\omega_1 + \varepsilon)t]\langle\langle A; V^{\omega_1}\rangle\rangle_{\omega_1} + \frac{1}{2}\int_{-\infty}^{\infty} d\omega_1 \int_{-\infty}^{\infty} d\omega_2 \exp[(-i(\omega_1+\omega_2) + \varepsilon)t]\langle\langle A; V^{\omega_1}, V^{\omega_2}\rangle\rangle_{\omega_1,\omega_2} + \ldots, \tag{4.7}$$

where the ω are frequencies of perturbations, and ε is an infinitesimal quantity that is set to zero after integration. The essential information of Eq. (4.7) is contained in the response functions. The linear response function

$$\langle\langle V^{\omega_0}; V^{\omega_1}\rangle\rangle_{\omega_1} = P(0,1)\sum_n \frac{\langle 0|V^{\omega_0}|n\rangle\langle n|V^{\omega_1}|0\rangle}{\omega_1 - \omega_n}, \tag{4.8}$$

is equal to second-order Rayleigh–Schrödinger perturbation theory when the perturbation is time-independent. Using the identity $V^{\omega_0} = A$, we have expressed the equation using $P(0,1)$, which means a sum over cyclic permutations of 0 and 1. Similarly the time-independent quadratic response function is

$$\langle\langle V^{\omega_0}; V^{\omega_1}, V^{\omega_2}\rangle\rangle_{\omega_1,\omega_2} = P(0,1,2)\sum_{nm} \frac{\langle 0|V^{\omega_0}|n\rangle\langle n|(V^{\omega_1} - \langle 0|V^{\omega_1}|0\rangle)|m\rangle\langle m|V^{\omega_2}|0\rangle}{(\omega_0 + \omega_n)(\omega_2 - \omega_m)}, \tag{4.9}$$

again with the permutation symbol $P(0,1,2)$. It should be noted that sums over states in the response functions described above are not necessary in practice and they can be replaced by tasks of solving linear systems of equations.

4.2.1 Isotropic nuclear magnetic shielding contributions

To evaluate the PV contributions to the NMR shielding tensor, and more specifically, to its isotropic part (which is independent of the molecular orientation), we will have to work out the response theory expressions that are bilinear in nuclear spin and external magnetic field (see Paper I). To do that, we will use the minimally substituted Hamiltonians of Eqs. (2.25)—(2.32).

First, we get a contribution from the PV Hamiltonian (2.29)

$$\sigma^{\mathrm{PV},d}_{K,\varepsilon\tau} = \frac{1}{\gamma_K} \sum_{\alpha} \varepsilon_{\varepsilon\tau\alpha} \langle h^{\mathrm{PV}(2)}_{KB_0,\gamma} \rangle. \tag{4.10}$$

Due to the anti-symmetric Levi–Civita symbol, this term does not contribute to the isotropic part of the tensor, which is what we are interested in. It should be also noted that Eq. (2.29) is proportional to $r_{i0}\delta(r_{iK})$, and can be completely excluded by placing the gauge origin O to the nucleus K. There is also a second term,

$$\sigma^{\mathrm{PV},p}_{K,\varepsilon\tau} = \frac{1}{\gamma_K} \langle\langle h^{\mathrm{PV}(2)}_{K,\varepsilon}; h^{\mathrm{OZ}}_{B_0,\tau} \rangle\rangle_0, \tag{4.11}$$

which is a combination of Eq. (2.28) and the orbital Zeeman (or angular momentum) term

$$\mathrm{H}^{\mathrm{OZ}}_{B_0} = \sum_{\alpha} h^{\mathrm{OZ}}_{B_0,\alpha} \mathrm{B}_{0,\alpha} \;\; ; \;\; h^{\mathrm{OZ}}_{B_0,\alpha} = \frac{1}{2} \sum_{i} \ell_{iO,\alpha}, \tag{4.12}$$

where ℓ_{i0} is the angular momentum operator of the electron i with respect to O. This term contributes also to the isotropic part and is the term that is going to be evaluated in the actual calculations.

As those are the only contributions of the order of αG_F and they both depend on the gauge origin, there is the question about the gauge independence of the combination of these terms. It can be shown that the combination is indeed gauge invariant at the complete basis set limit [37]. Neither of the contributions contains sum over nuclei, and if we assume that electrons are localized in the vicinity of nuclei, magnitudes of the contributions do not increase with the molecular size (shown numerically in Paper IV). Higher-order contributions (next being of the order of $\alpha^3 G_F$) can be obtained in a similar fashion, but they contain products of divergent operators, and thus are not well-behaved when the completeness of the basis set is increased. This is not a crucial problem if moderately sized contracted basis sets are used, and scalar relativistic and one-electron spin-orbit corrections have been evaluated in Paper II, and found to be useful.

As noted before, the parity-violating contributions to the NMR shielding constant split the resonance peak into two in a racemic mixture. This is illustrated in Figure 4.1, where it has been assumed that K is a spin-$\frac{1}{2}$ nucleus and

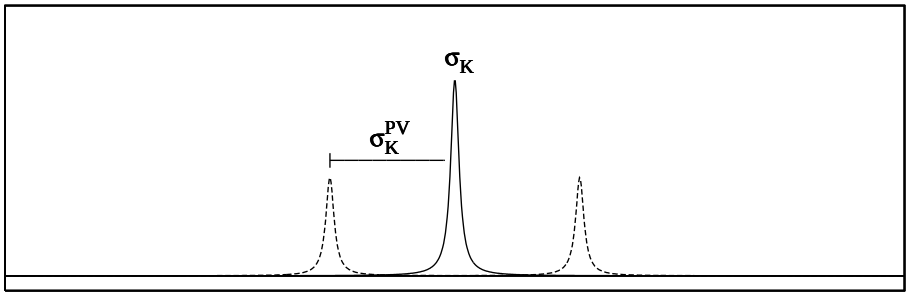

Figure 4.1: Illustration of the PV-induced split of the resonance peak of a spin-$\frac{1}{2}$ nucleus shielding constant.

there are no nuclear spin-spin couplings. The two peaks would correspond to parity-violation shifted peaks (shifted to opposite directions) of the two enantiomers.

4.2.2 Isotropic nuclear spin-spin coupling

Again, we are interested in isotropic contributions. The first leading-order ($\alpha^3 G_F$) contribution to the nuclear spin-spin coupling constant would be from Eq. (2.30) (see Paper I),

$$J^{\mathrm{PV},d}_{KL,\varepsilon\tau} = \frac{1}{2\pi}\sum_{\alpha}\varepsilon_{\varepsilon\tau\alpha}\langle h^{\mathrm{PV}(2)}_{KL,\alpha}\rangle, \tag{4.13}$$

but this one does not contribute to the isotropic part of the tensor. The next two contributions are obtained by combining the PV operator (2.32) with Fermi contact (FC) and spin-dipole (SD) operators,

$$\mathrm{H}^{\mathrm{FC}}_K = \sum_{\alpha} h^{\mathrm{FC}}_{K,\alpha}\mathrm{I}_{K,\alpha} \;;\; h^{\mathrm{FC}}_{K,\alpha} = \frac{4\pi}{3}\alpha^2 g_e\gamma_K\sum_i s_{i,\alpha}\delta(\mathbf{r}_{iK}), \tag{4.14}$$

$$\mathrm{H}^{\mathrm{SD}}_K = \sum_{\alpha\beta} h^{\mathrm{SD},\beta}_{K,\alpha}\mathrm{I}_{K,\alpha} \;;$$

$$h^{\mathrm{SD},\beta}_{K,\alpha} = \frac{1}{2}\alpha^2 g_e\gamma_K\sum_i s_{i,\beta}\frac{3r_{iK,\beta}r_{iK,\alpha} - \delta_{\beta\alpha}r^2_{iK}}{r^5_{iK}}, \tag{4.15}$$

where g_e is the electron gyromagnetic ratio. The contributions are the follow-

ing,

$$J^{\mathrm{PV,FC}}_{KL,\varepsilon\tau} = \frac{1}{2\pi}\sum_{\alpha}\left[\varepsilon_{\alpha\tau\varepsilon}\langle\langle h^{\mathrm{PV}(3)}_{K,\alpha\tau}; h^{\mathrm{FC}}_{L,\tau}\rangle\rangle_0 + \varepsilon_{\alpha\varepsilon\tau}\langle\langle h^{\mathrm{PV}(3)}_{L,\alpha\varepsilon}; h^{\mathrm{FC}}_{K,\varepsilon}\rangle\rangle_0\right], \quad (4.16)$$

$$J^{\mathrm{PV,SD}}_{KL,\varepsilon\tau} = \frac{1}{2\pi}\sum_{\alpha\beta}\left[\varepsilon_{\alpha\beta\varepsilon}\langle\langle h^{\mathrm{PV}(3)}_{K,\alpha\beta}; h^{\mathrm{SD},\beta}_{L,\tau}\rangle\rangle_0 + \varepsilon_{\alpha\beta\tau}\langle\langle h^{\mathrm{PV}(3)}_{L,\alpha\beta}; h^{\mathrm{SD},\beta}_{K,\varepsilon}\rangle\rangle_0\right] (4.17)$$

It turns out that the contribution in Eq. (4.16) has only non-diagonal elements, and although the term Eq. (4.17) has diagonal elements, their sum is zero due to the structure of the SD operator. Thus, neither of these terms contribute to the isotropic part of the spin-spin coupling tensor. The final leading-order contribution is

$$J^{\mathrm{PV},p}_{KL,\varepsilon\tau} = \frac{1}{2\pi}\left[\langle\langle h^{\mathrm{PV}(2)}_{K,\varepsilon}; h^{\mathrm{PSO}}_{L,\tau}\rangle\rangle_0 + \langle\langle h^{\mathrm{PV}(2)}_{L,\tau}; h^{\mathrm{PSO}}_{K,\varepsilon}\rangle\rangle_0\right], \quad (4.18)$$

which is a combination of Eq. (2.28) and the orbital hyperfine operator

$$\mathrm{H}^{\mathrm{PSO}}_K = \sum_{\alpha}\mathrm{I}_{K,\alpha}h^{\mathrm{PSO}}_{K,\alpha} \;\; ; \;\; h^{\mathrm{PSO}}_{K,\alpha} = \alpha^2\gamma_K\sum_i \frac{l_{iK,\alpha}}{r^3_{iK}}. \quad (4.19)$$

Contrary to the earlier terms, this term contributes to the isotropic part, and thus it will be the one used in calculations. None of these contain a reference to the gauge origin, and thus the gauge invariance is not a problem here. Again, higher-order contributions contain problematic delta-function terms, and even worse, some which are proportional to

$$\sum_N \delta(\mathbf{r}_{iN})\frac{\mathbf{r}_{iK}}{r^3_{iK}}, \quad (4.20)$$

which stems from Eq. (2.27). When this term is evaluated at $N = K$, it leads to an undefined expression $0/0$.

4.2.3 Electron spin-resonance g-tensor

The first PV contribution to the ESR g-tensor is the expectation value of the operator (2.26) (see Paper V),

$$\Delta g^{\mathrm{PV}(1)}_{\varepsilon\tau} = \frac{2}{\langle s^{\max}_z\rangle}\sum_{\alpha}\varepsilon_{\varepsilon\tau\alpha}\langle h^{\mathrm{PV}(1)}_{B_0,\alpha\varepsilon}\rangle. \quad (4.21)$$

The term $1/\langle s_z^{\max}\rangle$ is the spin-field reduction factor that is 1/2 for an open-shell doublet state [96]. In line with other expectation value contributions, Eq. (4.21) does not have an isotropic contribution. The other term is a combination of the orbital Zeeman interaction term and the PV contribution Eq. (2.25),

$$\Delta g_{\varepsilon\tau}^{\mathrm{PV}(2)} = \frac{2}{\langle s_z^{\max}\rangle}\langle\langle h_{\varepsilon}^{\mathrm{PV}(1)}; h_{\mathrm{B}_0,\tau}^{\mathrm{OZ}}\rangle\rangle_0. \tag{4.22}$$

A gauge invariant combination up to the order of αG_F is formed by (4.21) and (4.22). The proof is similar to that of the PV shielding contributions, and again, holds at the complete basis set limit. The PV Hamiltonian of Eq. (2.25) does not contain a reference to unknown λ-factors and this way PV *g*-tensor contribution evaluations would be more directly related to experiments than their NMR counterparts.

4.3 Electronic structure aspects of nuclear magnetic resonance parity-violation calculations

In this section, we will examine computational aspects of the evaluation of PV NMR contributions. Most of the benchmark results are from Paper II, but suitable results from other papers are also included.

4.3.1 Relativistic effects

Relativistic effects can be divided into two categories, scalar relativistic and spin-orbit effects. Scalar relativistic effects (SR) include spin-independent contributions such as the increase of the effective mass of a particle as its momentum increases. The spin-orbit interaction (SO) is the coupling of the spin of a particle with a magnetic field generated by the particle itself when it moves around the nucleus.

A series of dihedral molecules from H_2O_2 to H_2Se_2 form a simple hierarchy to test the sensitivity of the PV NMR contributions to the special rela-

Table 4.1: Impact of the treatment of relativistic effects as well as the model used for the nuclear charge distribution to the parity-violation-induced isotropic NMR shielding constant of selected nuclei in H_2O_2, H_2S_2, and H_2Se_2 at the HF level of theory using one-component (1-C) and four-component (4-C) wave functions. Two types of nuclear model are used, the point charge (PC) and the Gaussian models (GM). Results in 10^{-10} ppm.

	Wave function	Nuclear model	SR+SO	SR	NR
^{17}O	1-C(BP)	PC	29.17	30.13	29.12
	4-C	GM	31.67	34.05	32.90
	4-C	PC			32.86
^{33}S	1-C(BP)	PC	105.83	93.75	92.03
	4-C	GM	92.92	85.18	84.38
	4-C	PC			84.58
^{77}Se	1-C(BP)	PC	328.00	221.52	256.13
	4-C	GM	342.42	276.62	255.78
	4-C	PC			257.42

tivity. H_2O_2 and H_2S_2 contain only light elements, and therefore one would expect relativistic effects to be small. In H_2Se_2, on the other hand, selenium atoms are from the third row and it would be reasonable to expect at least some visible relativistic effects.

Relativistic effects can be significant as is shown in Table 4.1 (from Paper II). SR effects to the non-relativistic (NR) PV shielding contributions are not large, less than ten per cent, and are most pronounced in the ^{77}Se shielding constant (calculated at the HF level of theory). ^{77}Se is in this sense a light element and it has been shown that the SR effects increase in magnitude with $Z^{4.7}$ [38], where Z is the charge of a nucleus. The effects of special relativity in the PV contributions to the spin-spin coupling constants are shown in Table 4.2 (from Paper II), from which it can be seen that the spin-spin couplings contribution differ from the shielding contributions from the SR point of view. The SR effects are larger in proportion to magnitudes in couplings between the light elements than in the heavy element–heavy element coupling. For example, the difference in $J^{\mathrm{PV}}_{\mathrm{SeSe}}$ is less than ten per cent between the NR and SR results, whereas the same difference in $J^{\mathrm{PV}}_{\mathrm{OO}}$ is almost a factor of two.

Table 4.2: Effects of the relativistic treatment of parity-violation contributions to the spin-spin coupling constants of H_2O_2, H_2S_2, and H_2Se_2. Calculations were made at different levels of theory: four-component non-relativistic with point-charge nuclear model (NR-PC), and the following levels with Gaussian nuclear charge distribution: Four-component non-relativistic, four-component spin-free, and four-component Dirac–Coulomb Hamiltonians. All values in nHz.

Molecule	Coupling	SR+SO	SR	NR	NR-PC	1-C
H_2O_2	$^1J_{OH}$	0.0258	0.0233	0.0039	0.0212	0.0207
	$^2J_{OH}$	0.1265	0.1224	0.1086	0.1140	0.1094
	$^3J_{HH}$	0.0003	0.0003	0.0003	0.0003	0.0003
	$^1J_{OO}$	−0.5037	−0.4792	−0.8882	−0.3732	−0.4157
H_2S_2	$^1J_{SH}$	−0.0028	−0.0085	−0.0226	−0.0105	−0.0077
	$^2J_{SH}$	0.0433	0.0425	0.0354	0.0402	0.0385
	$^3J_{HH}$	0.0000	0.0000	0.0001	0.0001	0.0000
	$^1J_{SS}$	−0.1565	−0.2692	−0.3068	−0.2085	−0.2454
H_2Se_2	$^1J_{SeH}$	0.1378	−0.0256	−0.0495	−0.0172	−0.0190
	$^2J_{SeH}$	0.0041	0.0882	0.0546	0.0349	0.0778
	$^3J_{HH}$	−0.0002	0.0000	0.0000	0.0000	0.0000
	$^1J_{SeSe}$	12.9293	−8.2238	−7.5414	−9.2640	−6.6063

The SO interaction can also have large effects in heavy elements. In light elements containing molecules, H_2O_2 and H_2S_2, the spin-orbit interaction respectively decreases and increases the PV shielding contributions of the heaviest atoms of these molecules by 10 per cent. In H_2Se_2, the SO effect in the PV ^{77}Se shielding contribution is somewhat larger: It increases the contribution by 20 per cent as compared to SR results. By going further down in the H_2X_2 series to ^{125}Te and ^{209}Po, a Z^6 scaling of the SO effect at the Dirac–Hartree–Fock level of theory can be established [38]. PV spin-spin couplings are, again, more varying in their response to the SO effect. In H_2O_2, there are no large changes in contributions. In H_2S_2, the S–S coupling contribution is reduced by 42 % from its SR corrected value. In H_2Se_2, SO effects are rather dramatic. One of the the H–Se coupling contributions decreases in magnitude by 95 per cent, and the other H–Se coupling increases in magnitude by a factor of 5.5 and changes its sign. The largest of the PV contributions, $J^{\mathrm{PV}}_{\mathrm{SeSe}}$, changes its sign and increases in magnitude by approximately 60 per cent. Scaling of the SO effect to PV contributions in this property has not been

examined further, but large effects can be expected.

It is also possible to calculate relativistic corrections to PV contributions using the two-component non-relativistic limit as described in Paper I. Although this approach leads to some contributions that do not converge with respect to basis set size, it might still be instructive to evaluate them using medium-sized contracted basis sets to partially circumvent the problem. In Paper II, we evaluated selected contributions consisting of SR and one-electron SO corrections to the PV shielding contributions at the HF level of theory. The SO correction to the PV term should be well-behaved from the theoretical point of view. It gives corrections that are of the right sign but it slightly overestimates the magnitude. SR corrections work well in H_2O_2 and H_2S_2, but in H_2Se_2 the correction is too large and of the wrong sign. One should note that the SR contributions contain divergent terms, and therefore it is not so surprising that their relative performance is worse than that of SO corrections. The non-relativistic framework with SO corrections (which dominate the relativistic effects in heavy elements) can be useful for making cheap exploratory calculations.

4.3.2 Basis sets

Basis set effects in PV contributions to the NMR shielding constant have been examined in Figure 4.2 (from Paper II). Basis sets were cc-pwCVXZ (X = D, T, Q, 5) for ^{17}O and ^{33}S contributions, and cc-pVXZ (X = D, T, Q, 5) for ^{77}Se. Calculations were made using a range of electronic structure methods from HF to CC2 and CCSD (without the frozen core approximation), and several DFT exchange-correlation functionals. Convergence, in these cases, is not good. For example, results with cc-pwCVTZ basis set in ^{33}S contributions are off by more than a factor of two as compared to cc-pwCV5Z results, and no convergence is seen even at that level. Basis set effects are not that dramatic in H_2O_2, but convergence is still spurious. Convergence of different basis set families are shown in Figure 4.3 (from Paper II). There the cc-pVXZ and aug-cc-pVXZ basis sets, which are constructed from cc-pVXZ by adding extra diffuse functions, seem to converge much better than cc-pwCVXZ. The cc-

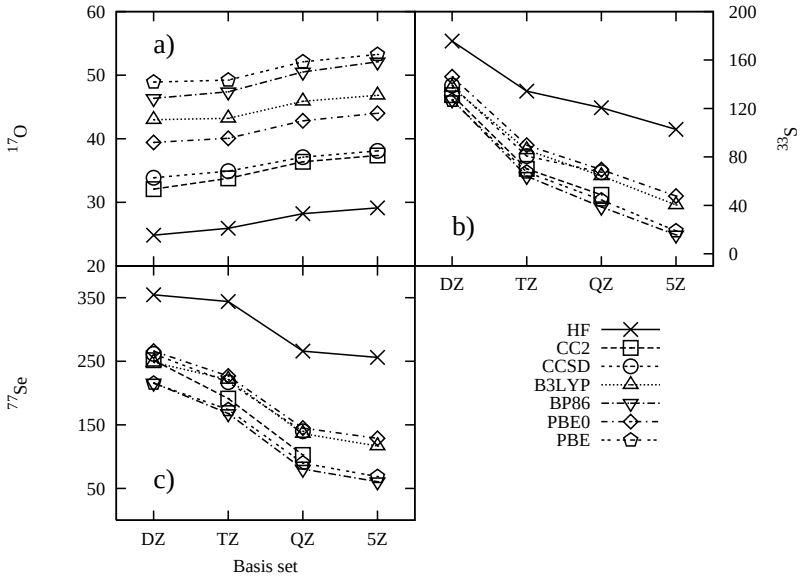

Figure 4.2: Basis set convergence of the PV shielding contributions using cc-pwCVXZ set for ^{17}O and ^{33}S and cc-pVXZ for ^{77}Se. All values in 10^{-10} ppm.

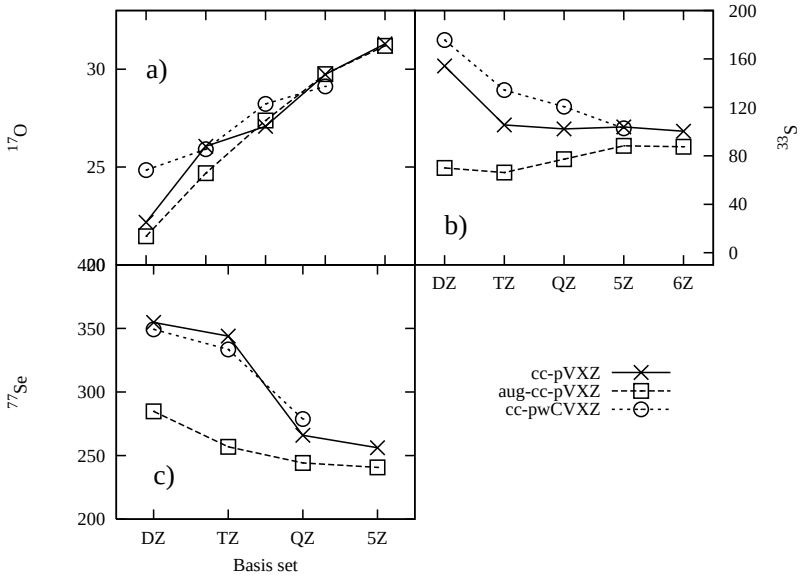

Figure 4.3: Convergence of the PV shielding contribution using different basis set families. All values in 10^{-10} ppm.

pwCVXZ basis sets are, on the other hand, much larger than the former and also include more core functions than cc-pVXZ and aug-cc-pVXZ basis sets.

In general, the wave function based correlation methods, CC2 and CCSD in this case, converge more slowly with respect to basis set size than the HF or DFT methods. This occurs because the Coulomb hole between electrons is only present in the correlated methods and its accurate description requires high angular momentum basis functions [50]. DFT should, in principle, also include the Coulomb hole but none of the current functionals properly describes it. However, the slow convergence of the PV contributions is thus most likely not due to the difficulties in describing the Coulomb hole. The cc-pwCVXZ basis set hierarchy increases the numbers of both valence and core basis functions when moving higher in the hierarchy. In this respect, valence regions should be well described with these functions, but the shortcoming in them is the incorrect description of regions close to nuclei. Gaussian basis sets need lots of steep functions to properly describe the core region. Basis sets designed for NMR properties, such as IGLO basis sets used in Papers I, IV and V, have a better description in that region than basis sets for general use, and thus the basis set convergence of PV properties is better. Similar conclusions have been drawn earlier by Laubender and Berger [36, 39]. They found out that adding steep *p*-type functions to Dunning's correlation consistent basis sets increases the rate of convergence significantly in HF and DFT calculations. Convergence of correlated calculations was also improved but not as much as in HF and DFT calculations. Similar results and conclusions also hold for spin-spin contributions (see Papers I and II).

4.3.3 Electron correlation

As for the basis sets, electron correlation effects can be benchmarked in a hierarchical manner. In Paper II, we have calculated PV contributions using wave function methods (HF, CC2, CCSD) and DFT using both GGA (BP86, PBE) and hybrid functionals (B3LYP, PBE0). The CC methods form a hierarchy in accuracy, as described in Chapter 3, and thus it is important to examine their results to obtain some idea of the magnitude of correlation effects. Even though our dihedral example systems are small and higher-order CC methods would, in principle, be applicable from a computational point of view, these

Table 4.3: Effects of electron correlation to the leading-order parity-violating contributions to the nuclear shielding constants (10^{-10} ppm) and indirect spin-spin couplings (nHz).

Molecule	Property	HF	CC2	CCSD	B3LYP	BP86	PBE0	PBE
H_2O_2	$\sigma^{PV}_{^{17}O}$	29.12	37.37	38.08	46.84	52.11	44.02	53.26
	$^1J^{PV}_{OH}$	0.0207	0.0156	0.0181	0.0232	0.0237	0.0227	0.0243
	$^2J^{PV}_{OH}$	0.1094	0.0881	0.0781	0.0982	0.0941	0.1009	0.0947
	$^3J^{PV}_{HH}$	0.0003	−0.0002	0.0006	0.0005	0.0005	0.0005	0.0005
	$^1J^{PV}_{OO}$	−0.4157	−0.3532	−0.3432	−0.4714	−0.4734	−0.4540	−0.4786
H_2S_2	$\sigma^{PV}_{^{33}S}$	92.03	43.11	60.00	35.50	13.18	42.20	16.13
	$^1J^{PV}_{SH}$	−0.0077	−0.0094	−0.0073	−0.0068	−0.0063	−0.0073	−0.0063
	$^2J^{PV}_{SH}$	0.0385	0.0458	0.0239	0.0410	0.0461	0.0453	0.0461
	$^3J^{PV}_{HH}$	−0.0000	−0.0001	−0.0000	−0.0000	−0.0000	−0.0000	−0.0000
	$^1J^{PV}_{SS}$	−0.2454	−0.1085	−0.1370	−0.1253	−0.0903	−0.1540	−0.0949
H_2Se_2	$\sigma^{PV}_{^{77}Se}$	256.13	102.59	139.86	116.78	60.54	128.64	68.57
	$^1J^{PV}_{SeH}$	−0.0190	−0.0272	−0.0184	−0.0118	−0.0101	−0.0147	−0.0101
	$^2J^{PV}_{SeH}$	0.0778	0.0952	0.0270	0.0631	0.0782	0.0824	0.0803
	$^3J^{PV}_{HH}$	−0.0000	−0.0002	−0.0001	−0.0000	−0.0000	−0.0000	−0.0000
	$^1J^{PV}_{SeSe}$	−6.6063	−2.5581	−3.1805	−3.0380	−1.9430	−3.7946	−2.0805

methods are rarely available with general purpose response theory modules. Therefore, we are forced to restrict our treatment up to the CCSD level with CC2 as an intermediate step. Depending on the molecule, CC2 and CCSD results can be close to each other as can be seen from Table 4.3. In H_2O_2, the difference in PV shielding contributions is on the order of one per cent while the CCSD correction to the HF value is almost 35 per cent. Because the CC2 and CCSD results are so close, an increase of 35 per cent in the magnitude of the ^{17}O PV shielding contribution is probably a good estimate for the role of electron correlation in this system. In H_2S_2 and H_2Se_2, electron correlation decreases the magnitude of PV contributions, and CC2 overestimates the correction by slightly less than 30 per cent as compared to CCSD while the overall correction approximately halves the HF values. Laubender and Berger performed similar studies with CC2 and CCSD using the same molecules but at fixed values of dihedral angles [39]. According to them, both CC methods gave values that differ less than 6 %, and differences between HF and CC results were smaller than in our study. Some of the difference could be explained by geometrical arguments. In particular, dihedral angles of our molecules (at the equilibrium geometry) are close to the zero-crossing of the PV contribution, and thus can be more sensitive to small differences. They also calculated PV contributions using the multi-configurational com-

plete active space SCF method, which was observed to underestimate the electron correlation effects compared to CC results, which are more suitable for simple closed-shell molecules.

Performance of the DFT functionals varies somewhat, but in general, both pure GGA functionals perform similarly and overestimate the correction radically. The hybrid functionals are also close to each other, and are better than pure GGAs. In H_2O_2, the overestimation effect is the largest, but in the two other molecules the hybrid functionals are close to CC2 in accuracy while pure GGA functionals give quite different results. The overestimation of the correlation effect by DFT functionals was also noted in Ref. [39], although only one GGA functional, BLYP, was used. The conclusions of Ref. [39] are not optimistic about the prospects of DFT, but our results show that hybrid functionals can produce results that are close to the CC results. This conclusion can also be supported by experience with other molecules, like CHFClBr and CHFBrI, where the PV contributions of both BLYP and B3LYP are close to each other (Paper I). This could imply that in some cases the general features of DFT work well for these kind of properties, although a firm statement can not be given from these examples alone.

Spin-spin coupling constant contributions seem to be much harder to describe for both CC and DFT methods. In H_2O_2, electron correlation (at the level of CCSD) reduces the magnitudes of all contributions slightly. Contrary to that, all DFT functionals increase the contributions by almost the same amount. In this property, there are no notable differences between hybrid and pure GGA functionals. A similar reduction can be seen in H_2S_2, but the magnitude of the effect is larger, and CC2 increases the magnitude of S–H coupling contributions. In the S–S coupling, the CC2 correction is of the right type but slightly too large. The performances of the CC methods for H_2Se_2 are similar to those for H_2S_2. All DFT functionals behave in a similar fashion and overestimate both ${}^2J^{\mathrm{PV}}_{\mathrm{SH}}$ and ${}^2J^{\mathrm{PV}}_{\mathrm{SeH}}$ couplings, and the values are somewhere between the HF and CC2 results. ${}^1J^{\mathrm{PV}}_{\mathrm{SH}}$ and ${}^1J^{\mathrm{PV}}_{\mathrm{SH}}$ DFT results are smaller in magnitude than the CCSD results. Heavy nucleus–heavy nucleus coupling contributions seem to be better described with B3LYP. The other hybrid functional, PBE0, underestimates the electron correlation effect, and both pure GGA functionals overestimate it.

In all molecules considered here, electron correlation plays a major role for PV contributions, and its inclusion is imperative for high-accuracy calculations. In H_2O_2, both CC2 and CCSD results are close to each other suggesting that CCSD could be close to the FCI limit. On the other hand, DFT performs worse for this molecule than for others, and both hybrid functionals seem to do better than pure GGAs. In the two other molecules, the discrepancy between CC2 and CCSD is large, and better *ab initio* methods would be needed for high-quality calculations. Again, hybrid functionals perform better than non-hybrid ones, although some failures can be seen.

4.3.4 Remarks on the combined effect

Examination of the combined effect of all three computational aspects described above would be time consuming. Relativistic Hamiltonians and their larger basis set requirements increase the number of degrees of freedom of the calculations significantly. For the CCSD calculations, computational scaling is o^2v^4, where o is the number of occupied and v is the number of virtual orbitals, so evaluation of PV contributions using high-level correlated methods becomes prohibitively expensive even for small molecules. Two-component approaches can handle larger molecules, but the performance of the current Breit–Pauli approach is not the best for heavy elements due to its non-optimal description of near nucleus relativistic effects. Other two-component methods, such as zeroth order regular approximation (ZORA), could provide a better description of the core, and the ZORA approach has been undertaken by Berger's group.

Effects of basis sets and electron correlation in the two-component framework are, in principle, simple to explore. However, a large basis set combined with a high-level *ab initio* electron correlation method is something where the converged limit has not yet been reached in PV properties. DFT, with hybrid functionals, is a good compromise between computational time and accuracy, although current functionals seem to systematically overestimate correlation effects. The good performance of the B3LYP functional is perhaps surprising as the functional is parametrized to reproduce thermochemistry well, but combined with a suitable basis set, it can guide the search for parity-violation in molecules.

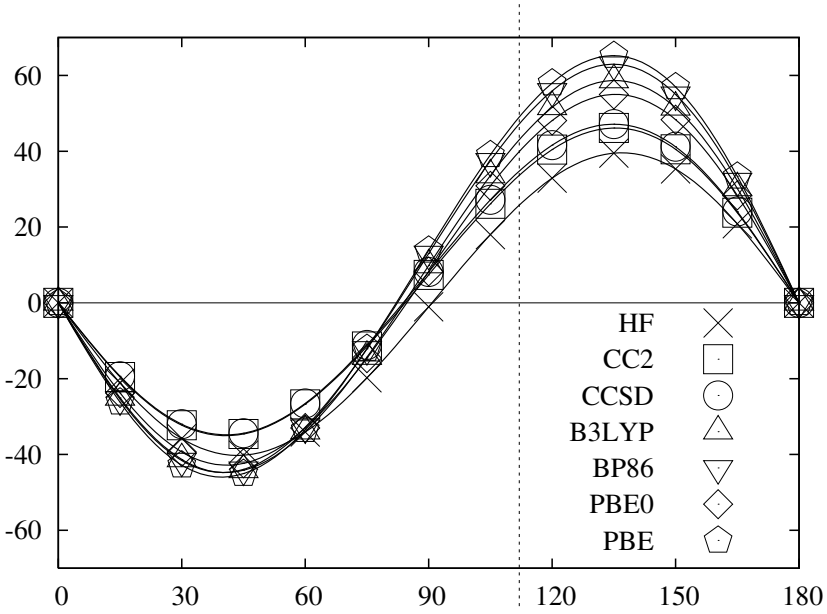

Figure 4.4: Dependence of the ^{17}O PV shielding contribution on the dihedral angle in H_2O_2 (in 10^{-10} ppm). Dotted line represents the equilibrium geometry.

4.4 Effects of molecular geometry on the PV NMR shielding constant

Our approach to molecular parity violation is based on the splittings of spectral peaks due to the different signs of contributions of mirror image molecules. When a chiral molecule becomes equivalent to its own mirror image, for example when the dihedral angle in H_2O_2 becomes 0° or 180°, the PV contribution vanishes. This is illustrated in Figure 4.4 (from Paper II), where the dependence of the PV contribution to the ^{17}O shielding constant on the dihedral angle is plotted using different electronic structure methods. It can be seen that the contribution goes to zero at the end points, 0° and 180°. Worth noting is also the asymmetric shape of the curve when correlated methods are used. HF values are scattered approximately in a symmetric fashion, but CC and DFT feature much larger values in magnitude in the range 90°–180°, and the zero crossing in the middle is shifted towards a lower value of the dihedral angle.

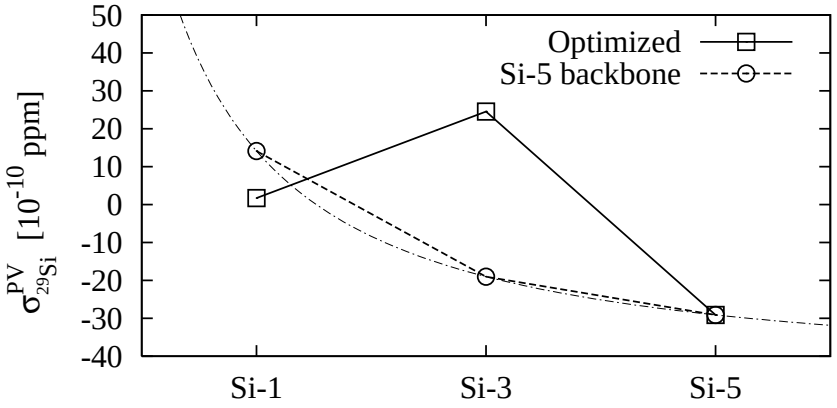

Figure 4.5: Dependence of the ^{29}Si PV contribution to the isotropic NMR shielding constant on the length of the Si-backbone and its structure.

4.4.1 Static geometry

Other examples of the geometry dependence can be found in Paper IV, where the PV contribution was evaluated for the ^{29}Si atom in a helical polysilyene. The polysilyene is composed of a silicon backbone with two side chains attached to each Si atom (see Paper IV for more details), and each side chain is a chiral alkane. The side chains had to be shortened to make a system with several Si atoms feasible for calculations, see Figure 4.6. The effect of side-chain truncation was examined by evaluating σ^{PV}_{Si} for three cases: fully optimized side chains, truncated but not optimized side chains and truncated side chains with a subsequent geometry relaxation. The difference between full side chains and truncated but not optimized was less than one per cent. When the truncated side chains were allowed to relax, the contribution was reduced by a factor of four, even though the structure near the Si atom changed little and the changes around chiral centers of side chains were also small. Figure 4.5 (from Paper IV) shows the dependence of the contribution on the surroundings of the Si atom. “Si-5 backbone” results were obtained by keeping dihedral angles between Si atoms from a backbone of five Si atoms and replacing the outermost Si atoms by hydrogens. If the structure was allowed to relax in shorter backbone lengths, even the sign of the contribution was not conserved. To account for variations like these, it is necessary to take molecular vibrations into account in a systematic way.

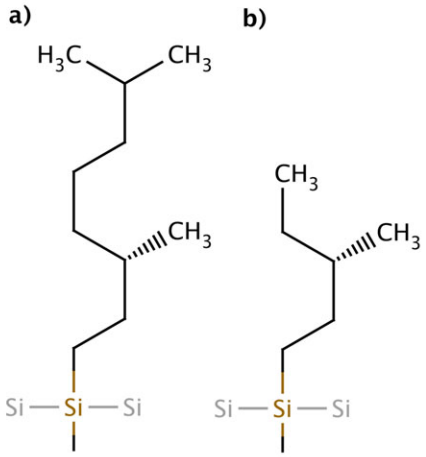

Figure 4.6: Side chains of the polysilyene: a) Full b) truncated.

4.4.2 Vibrational averaging

To take into account molecular vibrations, the vibrational methodology described in Chapter 3 is used in Paper III. Both VSCF and VCI methods for vibrational ground and excited states are used to explore the effect of vibrational averaging to the PV NMR shielding contributions. The CHFClBr molecule was chosen as a test system, because it is a rigid molecule with relatively heavy elements, and thus it is a good representative of a hypothetical experimentally realistic molecule. Although some of its vibrational modes are low in energy and thus easily excited, they consist of motions of heavy nuclei, and thus the variations in molecular geometry are small. At least they do not have a dramatic effect on the chirality and subsequently to the PV contributions, as compared to, e.g., the torsional motion of H_2O_2 (see Figure 4.4). Both potential energy and property surfaces were generated by single-point calculations using the B3LYP functional and the aug-cc-pVTZ basis set. The $64_1 16_1 4_1$ grid was also shown to be close to the convergence with respect to vibrational frequencies, which indicates that the PES is of good quality.

In Table 4.4, effects of different vibrational correlation methods and basis sets on to the PV contributions are investigated. It is seen that CHFClBr is a well-behaving molecule since there is little variance in results obtained with

Table 4.4: Vibrationally averaged ground state corrections to the PV contributions to the isotropic NMR shielding constants in CHFClBr using different vibrational correlation methods and basis sets. All values in 10^{-10} ppm.

	VCI[2]		VCI[3]		VCI[4]		
Nucleus	4HO	6HO	4HO	6HO	4HO	6HO	Ref.[a]
^{13}C	0.0353	0.0354	0.0358	0.0358	0.0358	0.0359	2.8732
^{1}H	0.0002	0.0002	0.0002	0.0002	0.0002	0.0002	0.0045
^{19}F	−0.0397	−0.0397	−0.0394	−0.0395	−0.0394	−0.0394	3.5870
^{35}Cl	2.0524	2.0544	2.0583	2.0603	2.0565	2.0585	−80.3963
^{79}Br	−1.5752	−1.5761	−1.5956	−1.5966	−1.5942	−1.5952	−52.7471

[a] Reference values calculated at the equilibrium geometry.

different methods and basis sets. The calculations were made using 2M4T property surfaces, which is of lower quality than the $64_1 16_1 4_1$ grid used for the PES. However, inclusion of three-mode couplings to the property surface changed the results by less than two per cent (not shown here). When comparing the VCI[4]/6 HO corrections to the reference values calculated at the equilibrium geometry, it is seen that the corrections are small. Vibrational corrections are of the order of a couple of per cents for the heavier nuclei. The largest correction, 4.5 %, is to the ^{1}H contribution, and the smallest corrections, approximately 1 %, are to the two other light elements. Similar corrections are also calculated for vibrationally excited states using the VCI[3]/6 HO combination, and the results are shown in Table 4.5.

Vibrational corrections to the PV contributions in vibrationally excited states are small when compared to the equilibrium geometry (Ref) reference results. However, some of the corrections to excited states are several times the value of the ground state (GS) correction. For example, the GS vibrational correction to the $\sigma_{Br}^{\mathrm{PV}}$ contribution is -1.6×10^{-10} ppm while the correction to mode ν_4 is -7.6×10^{-10} ppm. The latter value would be a 14 % correction to the reference value. Similar increases, as well as decreases, of magnitudes of corrections can be found from other excited states and for other nuclei. The most notable vibrational corrections can be found for the σ_{H}^{PV} contributions, where the correction can be up to 25 % of the reference value. For the room-temperature (300 K) measurements of PV effects, the most important vibrational states are perhaps the GS and modes ν_7–ν_9. Within this range of modes, vibrational corrections are within 5 % of the reference values. In

Table 4.5: Vibrational corrections to the parity violating contributions to the NMR shielding constants of nuclei in CHFClBr. Vibrational calculations were done at the VCI[3] level with the 6 HO basis set. All values in 10^{-10} ppm.

Mode	^{13}C	^{1}H	^{19}F	^{35}Cl	^{79}Br
Ref.[a]	2.8732	0.0045	3.5870	−80.3963	−52.7471
GS[b]	0.0358	0.0002	−0.0395	2.0603	−1.5966
ν_1	0.0576	0.0001	−0.1180	4.6371	−1.8024
ν_2	0.0307	0.0008	0.0478	−1.3839	−0.3128
ν_3	0.1875	−0.0003	−0.0953	6.1603	−5.5930
ν_4	0.1032	0.0004	−0.0379	5.8025	−7.5720
ν_5	−0.0394	−0.0000	−0.0761	0.5825	0.2025
ν_6	0.0442	0.0011	−0.0403	−1.4447	0.4571
ν_7	0.0180	−0.0006	−0.0782	3.1120	1.6706
ν_8	0.0637	0.0011	−0.0292	−2.7968	0.7138
ν_9	0.0659	−0.0000	0.0141	2.9577	−2.8544

[a] Reference value calculated at the equilibrium geometry.
[b] Vibrational correction to the ground state.

principle, it would be possible to pump molecules to a specific excited state (assuming that there would be enough intensity in the transition), but it is questionable whether the upsides (slightly increased PV contribution) would outweigh the downsides (such as many separated resonance peaks, relative loss of intensity etc.).

Table 4.6: Leading-order parity-violating contributions to electronic g-shift tensors of CH_3XHO (X = N, P, As, Sb). All values in ppm.

		Δg^{PV2}			
X	Method	g_{11}	g_{22}	g_{33}	g_{iso}
N	B3LYP	-1.20×10^{-10}	1.44×10^{-10}	-3.28×10^{-11}	-2.90×10^{-12}
	BP86	-1.33×10^{-10}	1.46×10^{-10}	-2.90×10^{-11}	-5.38×10^{-12}
	PW91	-1.19×10^{-10}	1.33×10^{-10}	-3.31×10^{-11}	-6.37×10^{-12}
P	B3LYP	-7.16×10^{-11}	-1.38×10^{-8}	1.49×10^{-8}	3.41×10^{-10}
	BP86	-4.11×10^{-10}	-1.32×10^{-8}	1.48×10^{-8}	4.13×10^{-10}
	PW91	-4.19×10^{-10}	-1.23×10^{-8}	1.39×10^{-8}	4.02×10^{-10}
As	B3LYP	7.07×10^{-8}	-2.59×10^{-7}	2.04×10^{-7}	5.18×10^{-9}
	BP86	6.36×10^{-8}	-2.54×10^{-7}	2.11×10^{-7}	6.83×10^{-9}
	PW91	6.11×10^{-8}	-2.44×10^{-7}	2.03×10^{-7}	6.88×10^{-9}
Sb	B3LYP	-1.78×10^{-7}	-4.46×10^{-6}	4.53×10^{-6}	-3.37×10^{-8}
	BP86	-1.59×10^{-7}	-2.59×10^{-6}	2.67×10^{-6}	-2.69×10^{-8}
	PW91	-1.62×10^{-7}	-2.18×10^{-6}	2.27×10^{-6}	-2.66×10^{-8}

4.5 Parity-violating effects in electron spin resonance

The theory of PV contributions to the g-tensor is presented in Paper V. The contributions are evaluated for four spin-doublet molecules, CH_3XOH, where X = N, P, As and Sb, using DFT with three density functionals, B3LYP, BP86 and PW91, and basis sets designed for magnetic resonance properties (IGLO-II–IGLO-IV).

The PV results obtained using the IGLO-IV basis sets are shown in Table 4.6. Both GGA functionals yield similar contributions depending slightly on the system and the basis set. B3LYP results with large IGLO-IV basis set are relatively close to to the GGA results, except in CH_3NOH, where discrepancies between functionals and basis sets are larger. Despite the variations between functionals, one can consider B3LYP calculations with the IGLO-IV basis set to be good enough for setting the scale of the PV contributions, because B3LYP works well for both the g-tensor and for the PV NMR contributions calculations. The magnitude range of the isotropic PV contributions is (in ppm) from 2.9×10^{-12} (CH_3NOH) via 3.2×10^{-10} (CH_3POH) and 5.2×10^{-9} (CH_3AsOH) to 3.4×10^{-8} (CH_3SbOH) when using the B3LYP functional with IGLO-IV basis set. It is easy to notice the similarity in mag-

nitudes of the PV g-tensor contributions to the non-relativistic NMR shielding contributions. While the magnitudes are similar, NMR resonance frequencies are in the MHz range in typical experiments whereas in ESR spectroscopy typical frequencies are in the GHz range. Remembering that our PV contributions are relative to "free" values (electron in ESR and ^{1}H nucleus in NMR), absolute splittings would be orders of magnitude larger in ESR than in NMR spectroscopy. Also, assuming that the magnitude of PV contributions is approximately proportional to the charge of the largest nucleus (although other factors are present, such as the difference between neutron and proton numbers of a nucleus), one would obtain a scaling factor of $Z^{4.3}$. Such a high scaling derived from non-relativistic calculations should be contrasted to the scaling of the corresponding NMR values, Z^2. For more rigorous scaling laws, relativistic effects, especially SO coupling, should be taken into account, preferably at the four-component level of theory.

5 Conclusions

In this thesis, I have discussed a mechanism of parity violation due to the electro-weak interaction. This mechanism results in small physical differences between mirror-image molecules, for example, the ground state energy of a left-handed molecule differs from the right-handed form. Examining this difference in molecular magnetic resonance properties was the main goal of this thesis.

The theory behind the parity violation (PV) was introduced in Chapter 2. Quantum field theory formalism was reduced to its low-energy limit, and further, using Foldy–Wouthuysen transformation, to a two-component form. Chapter 3 briefly introduced several methods of quantum chemistry, which were employed to evaluate the parity-violating contributions in Papers I-V. Based on the two-component form of the parity-violating mechanism presented in Chapter 2, explicit forms of the parity-violating contributions to the isotropic part of the nuclear magnetic shielding tensor, nuclear spin-spin coupling constant and electron spin resonance g-tensor were derived in Chapter 4.

Numerical estimates were presented in Chapter 4. PV contributions to the NMR shielding constants were in the range 10^{-6}–10^{-12} ppm in non-relativistic calculations (Papers I–IV and Ref. [36–39]), with an approximate Z^2 scaling with respect to the nuclear charge of the heaviest element. While relativistic effects do not have a dramatic effect on molecules containing (up to) third row elements (Paper II and Ref. [38]), the spin-orbit (SO) coupling can change the sign and increase the magnitude of a contribution in heavier elements by large amounts. For example, in H_2Po_2 the σ_{Po}^{PV} varies from -1.0×10^{-6} ppm (NR) to 1.3×10^{-3} ppm when all relativistic effects have been included [38], and the scaling of the PV effect increases to Z^6. Electron correlation has a significant effect on contributions, and it can increase (H_2O_2,

CHFClBr, CHFBrI) or decrease (H_2S_2, H_2Se_2) the contributions by approximately 50 % (Papers I and II and Ref. [39]). Basis set quality can have an even larger effect, and the difference between large and small basis sets can be more than a factor of two (Paper II and Ref. [39]). Similar benchmark calculations were made for nuclear spin-spin coupling constants (Papers I–II) and the PV contributions were in the range of 10^{-7}–10^{-11} Hz. Relativistic effects have more pronounced effects even in light element containing dihedral molecules than in the case of shielding contributions. Scalar relativistic effects do not play a large role, but the SO coupling changes the sign of the PV contribution already in H_2Se_2. Spin-spin coupling contributions are also very sensitive to basis set quality and electron correlation.

Vibrational corrections to the nuclear magnetic shielding contributions were found to be small in rigid molecules such as CHFClBr (Paper III). The size of the corrections did not have a systematic behavior as the largest vibrational corrections were for the σ_H^{PV} and the second largest for the $\sigma_{Br}^{\mathrm{PV}}$. In general, it was observed that the corrections were small, up to 5 % of the equilibrium geometry contributions including corrections from the low-energy vibrationally excited states. However, some of the corrections in vibrationally excited states were larger than the ground state corrections. For example, in ^{79}Br, the vibrational correction of mode ν_4 was approximately five times larger than the ground state correction, but their absolute magnitude was still smaller than 15 % of the total PV contribution.

In Paper IV, PV NMR shielding contributions were evaluated for helical polysilyene chains with a Si backbone and chiral alkane side chains. Although PV shielding contributions are size-intensive, as noted in Chapter 4, there were large variations in PV ^{29}Si shielding contributions with different Si chain lengths and types. However, the contribution seems to saturate at chain lengths longer than 5 Si atom. Fujiki used similar, although much longer, polysilyenes in an experiment [40], in which he found a difference in ^{29}Si shielding constants between the different enantiomers of the polysilyene chains. Such a splitting of a resonance between the enantiomers would be the way how the PV effects would appear in experiments. However, the observed difference was 0.06 ppm, which is several orders of magnitude larger than previous estimates using comparable, although smaller molecules. We estimated

the PV splitting to be of the order of 10^{-7} ppm and from the results, it is more than unlikely that the observed difference is due to the PV interactions.

All the PV NMR contributions evaluated in this thesis and in other references are below experimental accuracy. The largest PV contribution is to the NMR shielding of ^{209}Po in $H_2{}^{209}Po_2$, where a dihedral angle of 90° would induce a splitting of 6×10^{-6} ppm [38]. The results were calculated at the DHF level of theory without vibrational or electron correlation corrections. Taking into account our experience with lighter analogues, electron correlation might reduce the contribution by 50 %. Dihedral molecules are most likely more sensitive to vibrational corrections than CHFClBr because of the floppy motion, and thus the amount of correction is somewhat hard to estimate accurately based on the results of Paper III. However, based on the curve in Figure 4.4, it could be estimated that the vibrational corrections would be approximately 50 % at most. This would leave us with a perhaps optimistic splitting of roughly 1×10^{-5} ppm. If an NMR experiment on that system were possible in 21 T magnetic field (corresponding to 900 MHz ^{1}H frequency), the splitting of 10^{-5} ppm would then be equal to a splitting of 0.001 Hz for the ^{209}Po resonance peak. In principle, 1 mHz resolution could be achievable, but Polonium is not the most sensitive nucleus for NMR studies and there might be problems in preparation and isolation of the molecule.

If PV effects were seen in NMR experiments in the future, there are several parameters from which one could extract information, for example the Fermi coupling constant G_F, the Weinberg angle θ_W and nuclear factors λ_K. The first two have been measured accurately in high-energy experiments, but the λ factor has been measured convincingly only for the ^{133}Cs atom [31]. There have been experiments also on Thallium [97,98], but the results are not yet conclusive for nuclear anapole moments [32]. The focus of the experiments would be in very heavy elements, but inclusion of them in a molecule might also increase the PV effect of the other nuclei. For example, if ^{35}Cl in CHFClBr is substituted by a heavier ^{127}I to form CHFBrI, the σ^{PV}_{Br} is also increased by an order of magnitude. In this way, the range of nuclei on which information could be gathered could be increased substantially.

From the experimental point of view, however, the g-tensor of ESR spectroscopy could be more interesting than the NMR parameters. In Paper V,

we have presented theory and calculations for the PV contributions. Non-relativistic results were in the range of 10^{-12}–10^{-8} ppm with a scaling factor of Z^4 assuming that the of the contribution comes from the heaviest nucleus. Based on the experience on NMR properties, the inclusion of relativistic effects could increase the scaling factor significantly. Frequencies used in ESR experiments are also higher than in NMR experiments, and thus the absolute PV splittings would be larger than in the NMR case, even if the relative shifts were of the same order.

If the PV splitting in an ESR experiment could be observed, it could be used to obtain information on G_F, θ_W and Q_W. On the other hand, quantum chemical ESR calculations are challenging due to the open-shell nature of the molecules, and precise evaluations require expensive high-level multi-reference methods. Vibrational corrections would also have to be considered. Another drawback of using the g-tensor is its size-extensivity. At first sight, it might seem to be an advantage leading to an increased contribution, and hence easier detection. But for example, if one wants to extract $Q_W(Sb)$ from the CH_3SbOH g-tensor measurement, there are all the other Q_W factors included in the number. If one considers only molecules with one heavy nucleus, most of the contribution can be attributed to that, but then again, there is no additional help from other heavy nuclei. Weak nuclear charges have been measured accurately already (see, e.g., Ref [30] for a review), but to rule out theories beyond the Standard Model [99, 100], more accuracy is needed. That could perhaps be provided by ESR experiments.

In conclusion, in this thesis computational aspects of the PV contributions to the parameters of NMR and ESR spectrocopies have been surveyed with numerical estimates in some molecules. PV contributions are sensitive to all aspects of electronic structure calculations, but exploratory evaluations of contributions are possible for wide range of molecules. If a suitable candidate for experimental observation were found, accurate computations of contributions would be possible even though the computational cost of such calculations would be high. The remaining problem is to find suitable molecules that contain (several) heavy elements, are stable enough for experiments and can be synthesized in large enough quantities, a task which is not an easy one. Additional constraint for the experimental PV NMR shielding studies would

be the requirement for spin-$\frac{1}{2}$ nuclei so that the nuclear quadrupole moment would not further broaden the spectral peaks. If all the challenges were overcome, the study of PV effects in molecules would provide interesting new information about the fundamental interactions in nature.

Bibliography

[1] T. D. Lee and C. N. Yang. *Phys. Rev.*, 104:254, 1956.

[2] C. S. Wu, R. W. Hayward, D. D. Hoppes, and R. P. Hudson. *Phys. Rev.*, 105:1413, 1957.

[3] R. L. Garwin, L. M. Lederman, and M. Weinrich. *Phys. Rev.*, 105:1415, 1957.

[4] R. P. Feynman and M. Gell-Mann. *Phys. Rev.*, 109:193, 1958.

[5] E. C. G. Sudarshan and R. E. Marshak. *Phys. Rev.*, 109:1860, 1958.

[6] S. Weinberg. *Phys. Rev. Lett.*, 19:1264, 1967.

[7] J. K. Laerdahl, P. Schwerdtfeger, and H. M. Quiney. *Phys. Rev. Lett.*, 84:3811, 2000.

[8] H. Buschmann, R. Thede, and D. Heller. *Angew. Chem. Int. Ed.*, 39:4033, 2000.

[9] F. Faglioni, A. Passalacqua, and P. Lazzeretti. *Orig Life Evol. Biosph.*, 35:461, 2005.

[10] J. K. Laerdahl, R. Wesendrup, and P. Schwerdtfeger. *ChemPhysChem*, 1:60, 2000.

[11] R. Berger and M. Quack. *ChemPhysChem*, 1:57, 2000.

[12] R. Wesendrup, J. K. Laerdahl, R. N. Compton, and P. Schwerdtfeger. *J. Phys. Chem. A*, 107:6668, 2003.

[13] A. Salam. *J. Mol. Evol.*, 33:105, 1991.

[14] Y. Yamagata. *J. Theor. Biol.*, 11:495, 1966.

[15] D. K. Kondepudi and G. W. Nelson. *Phys. Rev. Lett.*, 50:1023, 1983.

[16] D. K. Kondepudi and G. W. Nelson. *Nature*, 314:438, 1985.

[17] R. Zanasi, P. Lazzeretti, A. Ligabue, and A. Soncini. *Phys. Rev. E*, 59:3382, 1999.

[18] W. Wang, F. Yi, Y. Ni, Z. Zhao, X. Jin, and Y. Tang. *J. Biol. Phys.*, 26:51, 2000.

[19] V. A. J. Avetisov, V. V. Kuz'min, and S. A. Anikin. *Chem. Phys.*, 112:179, 1987.

[20] R. Sullivan, M. Pyda, B. Wunderlich, J. R. Thompson, R. Pagni, H. Pan, C. Barnes, P. Schwerdtfeger, and R. Compton. *J. Phys. Chem. A*, 107:6668, 2003.

[21] R. G. Viglione, R. Zanasi, P. Lazzeretti, and A. Ligabue. *Phys. Rev. A*, 62:052516, 2000.

[22] M. Quack and J. Stohner. *Phys. Rev. Lett.*, 84:3807, 2000.

[23] P. Schwerdtfeger, J. K. Laerdahl, and C. Chardonnet. *Phys. Rev. A*, 65:042508, 2002.

[24] P. Schwerdtfeger, T. Saue, J. N. P. van Stralen, and L. Visscher. *Phys. Rev. A*, 71:012103, 2005.

[25] R. Berger and J. L. Stuber. *Mol. Phys.*, 105:41, 2007.

[26] Ch. Daussy, T. Marrel, A. Amy-Klein, C. T. Nguyen, Ch. J. Bordé, and Ch. Chardonnet. *Phys. Rev. Lett.*, 83:1554.

[27] J. Crassous, Ch. Chardonnet, T. Saue, and P. Schwerdtfeger. *Org. Biomol. Chem.*, 3:2218, 2005.

[28] F. Faglioni and P. Lazzeretti. *Phys. Rev. A*, 67:032101, 2003.

[29] W.-M. Yao and et. al. (Particle Data Group). *J. Phys.*, G 33:1, 2006.

[30] J. S. M. Ginges and V. V. Flambaum. *Phys. Rep.*, 397:63, 2002.

[31] C. S. Wood, S. C. Bennet, D. Cho, B. P. Masterson, J. L. Roberts, C. E. Tanner, and C. E. Wieman. *Science*, 275:1759, 1997.

[32] W. C. Haxton and C. E. Wieman. *Annu. Rev. Nucl. Part. Sci.*, 51:261, 2001.

[33] A. L. Barra, J. B. Robert, and L. Wiesenfeld. *Phys. Lett. A*, 115:443, 1986.

[34] A. L. Barra, J. B. Robert, and L. Wiesenfeld. *Europhys. Lett.*, 5:217, 1988.

[35] A. L. Barra and J. B. Robert. *Mol. Phys.*, 88:875, 1996.

[36] G. Laubender and R. Berger. *ChemPhysChem*, 4:395, 2003.

[37] A. Sonici, F. Faglioni, and P. Lazzeretti. *Phys. Rev. A*, 68:033402, 2003.

[38] R. Bast, P. Schwerdtfeger, and T. Saue. *J. Chem. Phys.*, 125:064504, 2006.

[39] G. Laubender and R. Berger. *Phys. Rev. A*, 74:032105, 2006.

[40] M. Fujiki. *Macromol. Rapid Commun.*, 22:669, 2001.

[41] O. Laporte and W. F. Meggers. *J. Opt. Soc. Am.*, 11:459, 1925.

[42] M. Bouchiat and C. Bouchiat. *J. Phys. (Paris)*, 35:899, 1974.

[43] R. A. Hegstrom, D. W. Rein, and P. G. H. Sandars. *J. Chem. Phys.*, 73:2329, 1980.

[44] M. Chaichian and N. F. Nelipa. *Introduction to Gauge Field Theories*. Springer-Verlag, 1984.

[45] S. A. Blundell, J. Sapirstein, and W. R. Johnson. *Phys. Rev. D*, 45:1602, 1992.

[46] L. L. Foldy and S. A. Wouthuysen. *Phys. Rev.*, 78:29, 1950.

[47] R. E. Moss. *Advanced Molecular Quantum Mechanics*. Chapman and Hall, London, 1973.

[48] Z. Gan and R. J. Harrison. Supercomputing, 2005. proceedings of the acm/ieee sc 2005 conference. page 22, 2005.

[49] F. Jensen. *Introduction to Computational Chemistry*. John Wiley & Sons, Chichester, second edition, 2006.

[50] T. Helgaker, P. Jørgensen, and J. Olsen. *Molecular Electronic-Structure Theory*. John Wiley & Sons, Chichester, 2000.

[51] P. Sałek, S. Høst, L. Thøgersen, P. Jørgensen, P. Manninen, J. Olsen, B. Jansík, S. Reine, F. Pawłowski, E. Tellgren, T. Helgaker, and S. Coriani. *J. Chem. Phys.*, 126:114110, 2007.

[52] J. Pople, M. Head-Gordon, and K. Raghavachari. *J. Chem. Phys.*, 87:5968, 1987.

[53] M. Kállay and J. Gauss. *J. Chem. Phys.*, 120:6841, 2004.

[54] T. Ruden, T. Helgaker, P. Jørgensen, and J. Olsen. *J. Phys. Chem.*, 121:5874, 2004.

[55] P. Hohenberg and W. Kohn. *Phys. Rev.*, 136:B864, 1964.

[56] W. Kohn and L. J. Sham. *Phys. Rev.*, 140, 1965.

[57] J. P. Perdew, A. Ruszinszky, J. Tao, V. N. Staroverov, G. E. Scuseria, and G. I. Csonka. *J. Chem. Phys.*, 123:062201, 2005.

[58] P. A. M. Dirac. *Proc. Cambridge. Phil. Soc.*, 26:376, 1930.

[59] J. C. Slater. *Phys. Rev.*, 81:385, 1951.

[60] D. M. Ceperley and B. J. Alder. *Phys. Rev. Lett.*, 45:566, 1980.

[61] S. H. Vosko, L. Wilk, and M. Nusair. *Can. J. Phys.*, 58:1200, 1980.

[62] J. P. Perdew. *Phys. Rev. B*, 33:8822, 1986.

[63] D. C. Langreth and M. J. Mehl. *Phys. Rev. B*, 28:1809, 1983.

[64] A. D. Becke. *Phys. Rev. A*, 38:3098, 1988.

[65] C. Lee, W. Yang, and R. G. Parr. *Phys. Rev. B*, 37:785, 1988.

[66] R. Colle and O. Salvetti. *Theoret. Chim. Acta*, 37:329, 1975.

[67] J. P. Perdew. *Electronic structure of solids '91*. Akademie Verlag, Berlin, 1991.

[68] J. P. Perdew, K. Burke, and M. Ernzerhof. *Phys. Rev. Lett.*, 77:3865, 1996.

[69] A. D. Becke. *J. Chem. Phys.*, 98:5648, 1993.

[70] P. J. Stephens, F. J. Devlin, C. F. Chabalowski, and M. J. Frisch. *J. Phys. Chem*, 98:11623, 1994.

[71] C. Adamo and V. Barone. *J. Chem. Phys.*, 110:6158, 1999.

[72] J. P. Perdew, M. Ernzerhof, and K. Burke. *J. Chem. Phys.*, 105:9982, 1996.

[73] B. Klahn and W. A. Bingel. *Theor. Chim. Acta*, 44:27, 1977.

[74] Dunning T. H., Jr. *J. Chem. Phys.*, 90:1007, 1989.

[75] D. E. Woon and Dunning T. H., Jr. *J. Chem. Phys.*, 98:1358, 1993.

[76] R. A. Kendall, Dunning T. H., Jr., and R. J. Harrison. *J. Chem. Phys.*, 96:6796, 1992.

[77] K. A. Peterson and Dunning T. H., Jr. *J. Chem. Phys.*, 117:10548, 2002.

[78] S. Huzinaga. *Approximate Atomic Functions*. University of Alberta, Edmonton, 1971.

[79] W. Kutzelnigg, U. Fleischer, and M. Schindler. *NMR Basic Principles and Progress*, volume 23. Springer, Berlin, 1990.

[80] Y. Shigeta, H. Takahashi, S. Yamanaka, M. Mitani, H. Nagao, and K. Yamaguchi. *Int. J. Quant. Chem.*, 70:659, 1998.

[81] M. Cafiero and L. Adamowicz. *Phys. Rev. Lett.*, 89:073001, 2002.

[82] T. Iordanov and S. Hammes-Schiffer. *J. Chem. Phys.*, 118:9489, 2003.

[83] H. Nakai. *Int. J. Quant. Chem.*, 107:2849, 2007.

[84] C. Eckart. *Phys. Rev.*, 47:552, 1935.

[85] J. K. G. Watson. *Mol. Phys.*, 15:479, 1968.

[86] Wilson B. E., Jr., J. C. Decius, and P. C. Cross. *Molecular Vibrations*. McGraw–Hill, New York, 1955.

[87] J. Kongsted and O. Christiansen. *J. Chem. Phys.*, 125:124108, 2006.

[88] A. Del Monte, N. Manini, L. G. Molinari, and G. B. Brivio. *Mol. Phys.*, 103:689, 2005.

[89] D. Toffoli, J. Kongsted, and O. Christiansen. *J. Chem. Phys.*, 127:204106, 2007.

[90] I. P. Hamilton and J. C. Light. *J. Chem. Phys.*, 84:306, 1986.

[91] O. Christiansen. *Phys. Chem. Chem. Phys.*, 9:2942, 2007.

[92] M. Kaupp, M. Bühl, and V. G. Malkin, editors. *Calculation of NMR and EPR Parameters: Theory and Applications*. Wiley-VCH, Winheim, 2004.

[93] P. Manninen and J. Vaara. *Phys. Rev. A*, 69:022503, 2004.

[94] J. Olsen and P. Jørgensen. *J. Chem. Phys.*, 82:3235, 1985.

[95] J. Olsen and P. Jørgensen. In D. R. Yarkony, editor, *Modern Electronic Structure Theory, Part II*. World Scientific, Singapore, 1995.

[96] J. E. Harriman. *Theoretical Foundations of Electron Spin Resonance*. Academic Press, New York, 1978.

[97] N. H. Edwards, S. J. Phipp, P. E. G. Baird, and S. Nakayama. *Phys. Rev. Lett.*, 74:2654, 1995.

[98] P. A. Vetter, D. M. Meekhof, P. K. Majumder, S. K. Lamoreaux, and E. N. Fortson. *Phys. Rev. Lett.*, 74:2658, 1995.

[99] M. Peskin and T. Takeuchi. *Phys. Rev. D*, 46:381, 1992.

[100] J. L. Rosner. *Phys. Rev. D*, 65:073026, 2002.